J Math Chem (2009) 45:563–597
DOI 10.1007/s10910-007-9344-5

ORIGINAL PAPER

The general concept of signal–noise separation (SNS): mathematical aspects and implementation in magnetic resonance spectroscopy

Dževad Belkić · Karen Belkić

Received: 13 November 2007 / Accepted: 27 November 2007 / Published online: 1 February 2008

Abstract Magnetic resonance spectroscopy (MRS) and spectroscopic imaging (MRSI) are increasingly recognized as potentially key modalities in cancer diagnostics. It is, therefore, urgent to overcome the shortcomings of current applications of MRS and MRSI. We explain and substantiate why more advanced signal processing methods are needed, and demonstrate that the fast Padé transform (FPT), as the quotient of two polynomials, is the signal processing method of choice to achieve this goal. In this paper, the focus is upon distinguishing genuine from spurious (noisy and noise-like) resonances; this has been one of the thorniest challenges to MRS. The number of spurious resonances is always several times larger than the true ones. Within the FPT convergence is achieved through stabilization or constancy of the reconstructed frequencies and amplitudes. This stabilization is a veritable signature of the exact number of resonances. With any further increase of the partial signal length N, towards the full signal length N, i.e., passing the stage at which full convergence has been reached, it is found that all the fundamental frequencies and amplitudes "stay put", i.e., they still remain constant. Moreover, machine accuracy is achieved here, proving that when the FPT is nearing convergence, it approaches straight towards the exact result with an exponential convergence rate (the spectral convergence). This proves that the FPT is an exponentially accurate representation of functions customarily encountered in spectral analysis in MRS and beyond. The mechanism by which this is achieved, i.e., the mechanism which secures the maintenance of stability of all the spectral parame-

Dž. Belkić (✉) · K. Belkić
Department of Oncology–Pathology, Karolinska Institute, P. O. Box 260, Stockholm, SE 17176, Sweden
e-mail: Dzevad.Belkic@ki.se

K. Belkić
Institute for Prevention Research, University of Southern California Keck School of Medicine, Los Angeles, CA 91803, USA
e-mail: Karen.Belkic@ki.se

ters and, by implication, constancy of the estimate for the true number of resonances is provided by the so-called pole-zero cancellation, or equivalently, the Froissart doublets. This signifies that all the additional poles and zeros of the Padé spectrum will cancel each other, a remarkable feature unique to the FPT. The FPT is safe-guarded against contamination of the final results by extraneous resonances, since each pole due to spurious resonances stemming from the denominator polynomial will automatically coincide with the corresponding zero of the numerator polynomial, thus leading to the pole-zero cancellation in the polynomial quotient of the FPT. Such pole-zero cancellations can be advantageously exploited to differentiate between spurious and genuine content of the signal. Since these unphysical poles and zeros always appear as pairs in the FPT, they are viewed as doublets. Therefore, the pole-zero cancellation can be used to disentangle noise as an unphysical burden from the physical content in the considered signal, and this is the most important usage of the Froissart doublets in MRS. The general concept of signal–noise separation (SNS) is thereby introduced as a reliable procedure for separating physical from non-physical information in MRS, MRSI and beyond.

Abbreviations

Ala	Alanine
AMARES	Advanced Method for Accurate Robust and Efficient Spectral fitting
Asp	Aspartate
au	Arbitrary units
BPH	Benign prostatic hypertrophy
Cho	Choline
Cr	Creatine
Crn	Creatinine
CT	Computerized tomography
FID	Free induction decay
FFT	Fast Fourier transform
FPT	Fast Padé transform
GABA	Gamma amino butyric acid
Glu	Glutamate
Gln	Glutamine
Glc	Glucose
GPC	Glycerophosphocholine
^{1}H MRS	Proton magnetic resonance spectroscopy
HLSVD	Hankel–Lanczos Singular Value Decomposition
Ins	Inositol
Iso	Isoleucine (Iso)
Lac	Lactate
LCModel	Linear Combination of Model in vitro Spectra
Lip	Lipid
Lys	Lysine
Met	Methionine

MR	Magnetic resonance
MRI	Magnetic resonance imaging
MRS	Magnetic resonance spectroscopy
MRSI	Magnetic resonance spectroscopic imaging
ms	Milliseconds
NAA	*N*-acetyl aspartate
NAAG	*N*-acetyl aspartyl glutamate
NMR	Nuclear magnetic resonance
PA	Padé approximant
PCho	Phosphocholine
PCr	Phoshocreatine
PET	Positron emission tomography
ppm	Parts per million
PSA	Prostate specific antigen
RT	Radiation therapy
SNR	Signal-to-noise ratio
SNS	Signal–noise separation
Tau	Taurine
TE	Echo time
Thr	Threonine
Val	Valine
VARPRO	Variable Projection Method
ww	Wet weight
1D	One dimensional
2D	Two dimensional

1 Introduction

1.1 Increasing appreciation of magnetic resonance spectroscopy as a potentially key modality for cancer diagnostics

Magnetic resonance (MR)-based methods are becoming the modality of choice for a rapidly expanding range of applications in oncology. Magnetic resonance imaging being non-invasive, highly sensitive and free from ionizing radiation is indispensable for timely detection of many cancers. However, magnetic resonance imaging (MRI) often has poor specificity. Molecular imaging through magnetic resonance spectroscopy (MRS) and spectroscopic imaging (MRSI) can enhance specificity by detecting metabolic features characteristic of malignancy. Also, molecular changes often precede morphologic alterations, so that sensitivity can be further improved by MRS and MRSI. This kind of molecular imaging is becoming widely appreciated as an extraordinary opportunity for early detection, by identifying key changes for the emergence and progression of cancer on the molecular level.

An example of how MRS can improve the specificity of MRI is provided in Fig. 1. On the left panel two hyperlucent lesions are observed via T_2 weighted MRI. These two lesions were practically indistinguishable, even with contrast enhancement

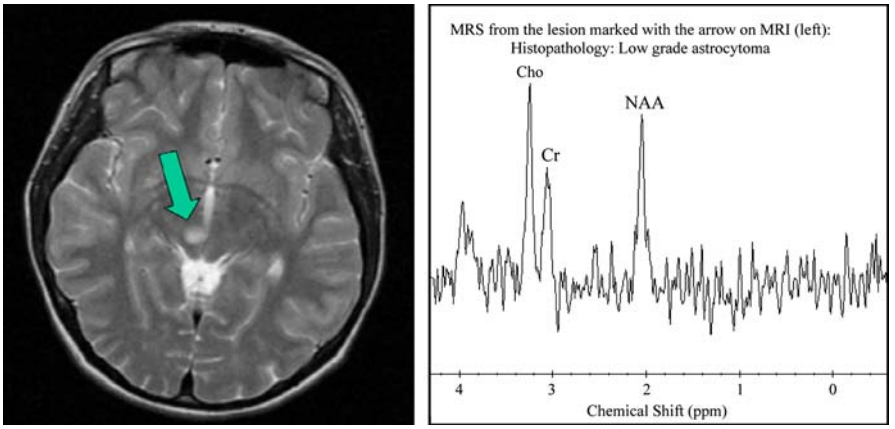

Fig. 1 *Left panel*: T_2 weighted MRI shows two, very similar appearing hyperlucent lesions. *Right panel*: spectrum obtained via MRS from the lesion marked with the *arrow* in the *left panel*. The high ratio of choline (Cho) to creatine (Cr) and of choline to *N*-Acetyl-Aspartate (NAA) suggested malignancy. Histopathology confirmed this, with the finding of a low grade-astrocytoma. The abscissa on the right panel is chemical shift as a dimensionless frequency in parts per million (ppm), whereas the ordinate is intensity in arbitrary units (au). Chemical shifts indicate the frequencies at which various metabolites resonate to the external excitation. Adapted from: Dr. Erik Akkerman, Academic Medical Center, Amsterdam (private communication)

(not shown). The metabolic information provided by MRS (right panel) suggested that only the lesion with the arrow was malignant, and this was subsequently confirmed with a histopathologic diagnosis of low-grade astrocytoma.

In the recent period, striking attention has been paid in leading investigative clinical journals to in vivo MRS as a potentially key non-invasive modality for cancer diagnostics [1–13]. The combination of anatomic localization and metabolic information is often decisive for identifying cancer, especially since metabolic changes can often precede anatomic/morphologic alterations. This can be invaluable, especially in difficult cases, e.g., differentiating recurrent tumor from radiation necrosis or post-operative changes [12,14]. These advantages have become particularly clear for neuro-oncology [4,9,13,15–17] and prostate cancer diagnostics [5,6,9,10,18]. Accuracy of breast cancer detection and prediction of response to chemotherapy have been improved by MRS, in combination with contrast-enhanced MRI [2,3,9,11,19–21]. MRS has also increased diagnostic accuracy for other malignancies e.g., thyroid [8] and other types of head and neck cancers [1,7]. Spectroscopic information from fine needle aspiration of biopsy specimens has also been found to provide rapid and quite accurate detection of metastatic melanoma in lymph nodes [22]. Moreover, as a non-invasive method with the possibility of full volumetric coverage, MRSI can provide vital information when biopsy is not possible due to potential morbidity. This is particularly the case in brain tumor diagnostics, where MRS and MRSI are virtually irreplaceable.

Notwithstanding these achievements, there are still important shortcomings of current applications of MRS to clinical oncology, that have hampered wider implementation of this method in cancer diagnostics.

Very few of the metabolite concentrations or their ratios estimated in the conventional way unequivocally distinguish tumors from normal tissue, nor are these specific for cancer. For example, infection, infarction and demyelinating disorders frequently show spectral changes identical to those of brain tumors. Histopathological characterization and brain tumor grading have been greatly aided by MRS. Nevertheless, there are numerous contradictory findings in the literature. Particularly troublesome is the limited possibility of MRS to detect very small tumors. For breast cancer diagnostics using MRS, this is especially problematic, due to the need for lipid suppression. A current strategy has been to increase echo time (TE), to decrease overlap with lipid signal, but this is achieved by a diminution in signal intensity. Also, metabolites with short T_2 relaxation times will have decayed at longer TE; e.g., myoinositol whose estimated concentrations best distinguished breast cancer from a fibroadenoma in our analysis [23,24] of in vitro MRS data [25]. Poor signal to noise ratio (SNR) is a major cause of false negative findings using MRS to detect malignant breast lesions [26]. Breast cancer detection through MRS has mainly relied upon the presence or absence of a composite (total) choline peak. This compromises diagnostic accuracy, since choline may be observed in benign breast lesions and in normal breast during lactation. Furthermore, choline is often undetected in small tumors that are then misclassified as benign [26].

Metabolite ratios are also problematic, being dependent upon TE [27], and affected by confounding factors including cancer treatment itself. Consequently, malignancy-defining ratio cut-points vary widely from author to author [14]. Even for prostate cancer diagnostics where choline-to-citrate ratios are of major help, dilemmas often arise. For example, in stromal tissue or metabolic atrophy, citrate levels are low without cancer being present, while with prostatic hypertrophy, citrate can still be high despite coexistent malignancy [14].

For detecting tumors in deep-seated, moving organs applications of MRS are hampered by poor SNR [28]. A case in point is the ovary where early cancer detection is still beyond current reach. Because of the small size and motion of this organ, in vivo MRS is mired by problems of resolution and SNR, and yet, there is a rich store of MR-observable compounds that distinguish benign from cancerous adnexal masses when in vitro MRS with its attendant high resolution is applied [29–32]. It has been suggested that insofar as the current problems hindering encoding of high quality time signals are overcome, in vivo ^{1}H MRS could become the method of choice for evaluating ovarian lesions [32].

1.2 Optimization of MRS for improved cancer diagnostics needs more advanced signal processing methods

As will be described in the next sub-section, many problems with current applications of MRS within clinical oncology are directly related to reliance upon the conventional signal processing method, i.e., the fast Fourier transform (FFT). Optimization of MRS for timely cancer detection requires more advanced signal processing. One may wonder: how could mathematics play such a critical role in medical diagnostics? This is because data encoded directly from patients by means of existing imaging techniques,

e.g., CT (computerized tomography) or PET (positron emission tomography), as well as MRI [33,34] and MRS [35,36] are not at all amenable to direct interpretation, which therefore need mathematics via signal processing. Global strategies along these lines, intertwining signal processing with quantum mechanics and mathematical modeling are detailed in [35,37].

Figure 2 provides a graphic illustration of why mathematical methods are absolutely vital for MRS. The top panel of this figure shows the recorded data, called a time signal or free induction decay (FID). The abscissa is time in milliseconds (ms) and the ordinate is the strength (intensity) of the signal in arbitrary units (au). This FID is a heavily packed oscillating signal whose intensity decays exponentially over time. However, not even the trained eye of the most astute clinician could decipher much meaningful information directly from the time signal. Yet, from this time signal the MR spectrum is obtained, with its clear advantage of depicting a relatively small number of distinct features that are then more amenable to direct theoretical analysis and interpretation. Such a spectrum is displayed on the middle panel via the total absorption shape spectrum.[1] This is obtained by a mathematical transformation of the time signal into its complementary (dual) representation, in the frequency domain. Here, as alluded to above, more discernable information is provided. This total shape spectrum provides qualitative information about the sum of metabolites, but not their components. Therefore, while more revealing than the time signal, the output data is still qualitative and inconclusive. Note that the customary data analytical techniques, i.e., the FFT, take us only to this second step—the total shape spectrum (envelope).

In other words, from the absorption total shape spectrum on the middle panel of Fig. 2, more information is needed before the metabolites can be identified and their concentrations reliably determined. Namely, how many metabolites underlie each peak in the total shape spectrum and what is the relative strength of each of these components? From the shape spectrum, this information can only be guessed, as customarily done by various fitting algorithms used in the MRS literature. However, more advanced mathematical methods, such as the FPT, are needed to achieve this vital next step with certainty. In the lower panel of Fig. 2, the components are shown immediately under the total shape spectrum. It is clearly seen that sometimes two, three or even more peaks underlie a given structure, and each of these peaks can, in principle, represent a metabolite.[2] In the next sub-sections, we will explain how the fast Padé transform unequivocally provides this key information for MRS, which has been lacking with customary data analytical techniques.

The strategic importance of robust and uniform data processing of MRS signals has been strongly emphasized [3,38] at e.g., the expert meeting on MRS for oncology, held recently by the US. National Cancer Institute [3], as well as at a special conference in November 2006 on Data Processing in MR Spectroscopy and Imaging by the International Society for Magnetic Resonance in Medicine (www.ismrm.org/workshops/datao6/index.htm).

[1] The absorption spectrum is the real part of the corresponding complex-valued spectrum.

[2] Each metabolite, being a molecule, can have more than one resonance.

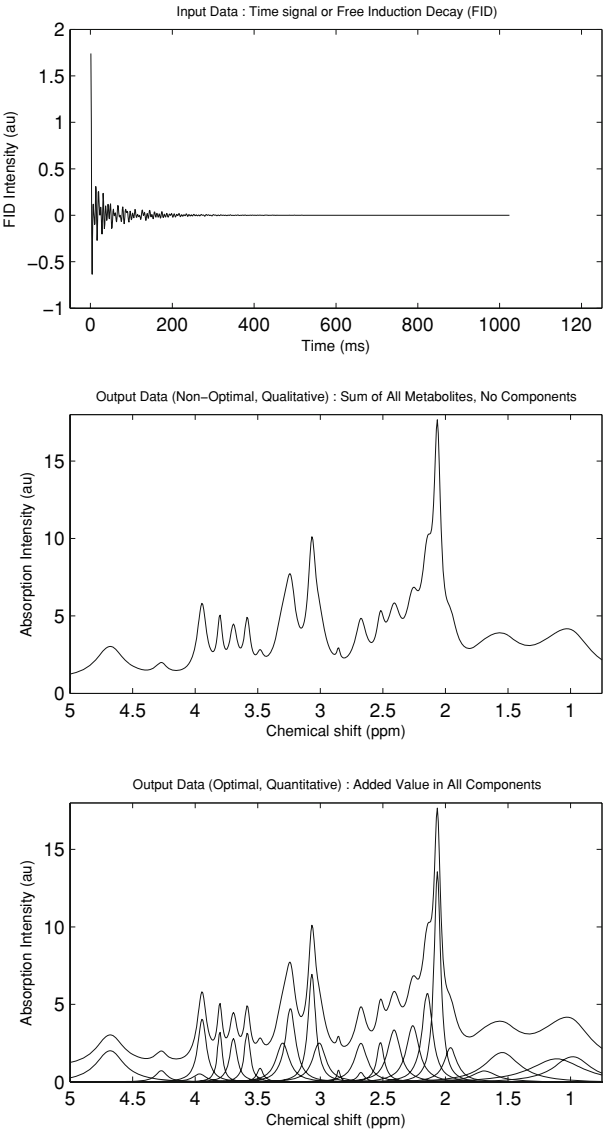

Fig. 2 *Top panel*: time signal or FID. The *middle panel* is the absorption total shape spectrum. The *lower panel* shows the absorption total shape spectrum and the underlying component shape spectrum

1.3 Customary (non-optimal) data analytical techniques used in MRS

The most commonly used analytical technique in MRS is the fast Fourier transform. The FFT has been widely used for data processing in the clinical setting because of its steady convergence with increasing signal length N at a selected bandwidth (or equivalently, with increasing total acquisition time T), such that reasonable looking

MR shape spectra are obtained for not so severely truncated time signals.[3] This steady convergence means that there are no major troublesome surprises for varying T. In sharp contrast, nearly all parametric estimators show marked instability as a function of the signal length. This is manifested in dramatic oscillations (e.g., spikes and other artificial spectral structures) that appear prior to convergence (if at all), as pointed out in Refs. [35,36]. Needless to say, such spurious findings are anathema to the clinical demands for reliable spectral information aimed at aiding diagnostics. Although computationally stable, the FFT only estimates the total shape of the spectrum, and does so with low-resolution, which is equal to $2\pi/T$.

Within the FFT, a complex-valued Fourier spectrum is defined by using only *a single polynomial*:

$$F = \frac{1}{N}\sum_{n=0}^{N-1} c_n e^{2i\pi nk/N}; \quad 1 \le k \le N-1, \tag{1}$$

with pre-assigned angular frequencies, whose minimal separation $2\pi/T$ is determined by the total acquisition time $T = N\tau$, where τ is the sampling time (inverse of the chosen bandwidth). The FFT spectrum is defined *only* on the Fourier grid points $2\pi k/T (k = 0, 1, \ldots, N-1)$.

The strategy applied in attempts to improve resolution has been to increase T and thereby decrease the distance $2\pi/T$ between adjacent gridpoints. This does not solve the problem at all, because MRS signals become heavily corrupted with background noise at longer T. Since these time signals decay exponentially as an FID (see top panel of Fig. 2), larger signal intensities are observed early in the encoding. It is, therefore, advantageous to rapidly encode FIDs, avoiding long T at which mainly noise is measured. Thus, there are two mutually exclusive requirements within the FFT whose attempts to improve resolution lead to worsened SNR. The FFT is a linear transform, and, as such, imports noise as intact from the time to the frequency domain, further contributing to poor SNR [35]. Moreover, the FFT has no extrapolation property based upon the encoded FID.

The FFT is limited to non-parametric estimation, providing only the total shape or envelope of spectral structures, *but not their number or quantification*. Peak parameters are subsequently extracted in post-processing by fitting, which is non-unique. This means that e.g., 2, 3 or more resonances can yield the same fit to a given structure, with no way to tell which of the fits is correct, as reminiscent of the famous Lanczos example [39,40]. This can be inferred from Fig. 2 (bottom panel). These problems are most pronounced for overlapping resonances, which are often clinically important [41]. Many contradictory findings in tumour diagnostics are related to whether or not a given metabolite was included in the original expansion basis set [42,43], as in the Linear Combination of Model in vitro Spectra (LCModel) [44]. Besides the fact that fitting is non-unique, much information contained in the signal is not obtained in an

[3] In practice, all experimental time signals are truncated, since infinitely long signals required by the exact Fourier analysis cannot be measured. This is not critical for relatively long signals, but considerable spectral deformation (e.g., Gibbs ringing, etc.) can arise for severe truncations.

adequate way, such that estimates for position, width, height and phase of resonances can be biased [35]. Metabolite concentrations can only be accurately computed if these parameters are obtained in a reliable way with an intrinsic and robust error analysis. The vital need for this quantitative information in cancer diagnostics has been repeatedly underscored with respect to MRS [14,26,32,39,45,46].

1.4 Novel (optimal) data analytical methodologies, the fast Padé transform (FPT): specific relevance for MRS in cancer diagnostics

1.4.1 Improved resolution and signal to noise ratio of the FPT

In recent publications [35,36,47–52], it has been conclusively demonstrated that high resolution methods, notably the fast Padé transform, the FPT as it is acronymed, can overcome many of the above-described limitations of the FFT, that hamper further progress of MRS in cancer diagnostics. The FPT is a non-linear *polynomial quotient* P_L/Q_K of the exact finite-rank spectrum (Green function) given by the Maclaurin series with the encoded raw time signal $\{c_n\}$ as the expansion coefficients. Non-linearity of the FPT yields noise suppression. The FPT shares the FFT's most favorable property, i.e., the FPT is a stable processor when signal length is systematically augmented at a fixed bandwidth, producing no spikes or other spectral deformations [35,52]. In contrast to the FFT, it is known that the FPT is a powerful interpolator and extrapolator [35]. Due to extrapolation, which is present in the implicit polynomial inversion via Q_K^{-1} in P_L/Q_K, inference is gained from a non-measurable infinite number of signal points by using only the available finite set $\{c_n\}$ $(0 \leq n \leq N-1, N < \infty)$. The FPT can use the fixed Fourier mesh $2\pi k/T$ $(k = 0, \ldots, N-1)$, but this is not mandatory, as opposed to the FFT. In other words, the FPT can be computed at any frequency ω. Unlike the FFT, resolution in the FPT is not pre-determined by T. Moreover, due to its parametric estimation and extrapolation capabilities, the FPT has a much better resolving power than the FFT.

Rapid convergence, improved SNR and resolution, plus robust error analysis yield markedly enhanced information content extracted by the FPT from in vivo MRS signals, relative to the FFT, as demonstrated in Refs. [36,47,48,52] via detailed comparisons of the FPT and FFT using clinical in vivo MRS FIDs. Further improvements in resolution by reducing Gibbs ringing have also been achieved [53]. Crucially, unique to the FPT is its unprecedented capability to unequivocally identify and separate noise from the genuine/physical content of the signal by using the powerful concept of Froissart doublets (pole-zero cancellations) [50,51]. In Refs. [36,47–49,52,54], we applied the FPT to in vivo MRS FIDs [55] of brain occipital grey matter recorded from healthy volunteers at high magnetic field strength (4T and 7T). These FIDs are long ($N = 2048$) with excellent SNR, so that the total shape spectra from the FFT with all N points served as gold standard. In Refs. [36,54], we demonstrated that at any level of truncation of the full signal length N at a fixed bandwidth, the clinically relevant resonances that determine concentrations of metabolites in the investigated tissue are significantly better resolved in the FPT than in the FFT. In particular, the FPT can achieve the same resolution as the FFT by using twice shorter time signals.

Self-contained verification of all the results from the FPT is secured by using two conceptually different, but nevertheless equivalent algorithms. These are the two variants of the FPT, initially defined inside ($|z| < 1$) and outside ($|z| > 1$) the unit circle, but extended automatically to the whole complex frequency plane by the Cauchy analytical continuation principle. The difference between the converged spectra from these two variants of the FPT coincides with the experimental background noise level. This represents one of the intrinsic cross-validations of the findings and robust error analysis of the FPT without relying upon the FFT or any other estimator [48,52]. For establishing the validity of parametric methods, error analysis is of critical importance.

In Fig. 3 adapted from Ref. [50] we compare the performance of the FPT and the FFT for high-resolution absorption total shape spectra. These spectra correspond to an FID typically encoded clinically from a healthy human brain via MRS using an external static field $B_0 = 1.5$ T and a short TE of 20 ms, with total length $N = 1024$ and bandwidth 1000 Hz so that $\tau = 1$ ms (see e.g., [56]). Resolution and convergence rates are clearly seen in Fig. 3 to be much better in the FPT than the FFT at any partial signal length $N_P = N/M (M > 1)$. Especially striking is that already at one eighth of the signal length ($N/8 = 128$), the FPT almost completely reflects the converged spectrum, whereas the FFT requires the total signal length N to achieve full convergence. This markedly enhanced resolution capacity of the FPT can be of vital clinical importance in cancer diagnostics, as demonstrated, with respect to distinguishing malignant versus benign ovarian lesions [57,58].

1.4.2 Exact quantification by the FPT

Notwithstanding interest in the initial studies for MR absorption total shape spectra using the FPT [36,52], the primary goal in the related most recent publications [50,51,59,60] has been to go one critical step further by explicitly reporting the numerical/tabular results via reliable quantification in MRS. In other words, we have sought to go beyond the qualitative information on shape spectra, to provide the actual spectral components, i.e., the optimal, quantitative information, the importance of which was illustrated by the example in Fig. 2. In [37,50,51] it is described, in detail, how the FPT unequivocally reconstructed the spectral parameters, so that the component spectra could be generated for all the physical resonances from time signals similar to those recorded in clinical scanners. In Refs. [35,50,51,54] validation is provided for the powerful computational algorithms by which the FPT yields quantitative spectral parameters. This is done without fitting and the solution is *unique*. Moreover, the FPT also outperforms other parametric estimators as well as fitting techniques used in MRS, such as HLSVD (Hankel–Lanczos Singular Value Decomposition) [61], VARPRO (Variable Projection Method) [62], AMARES (Advanced Method for Accurate Robust and Efficient Spectral fitting) [63], and LCModel [44], etc.

These studies represent a critical step forward for signal processing in MRS, with particular relevance to clinical oncology, due to the unprecedented capability of the FPT to unambiguously resolve and quantify all the physical resonances. There is an urgent need for accurate quantification to determine metabolite concentrations, so that MRS can be better used to detect and characterize cancers, with clear distinction from non-malignant processes. Metabolite concentrations can only be accurately computed

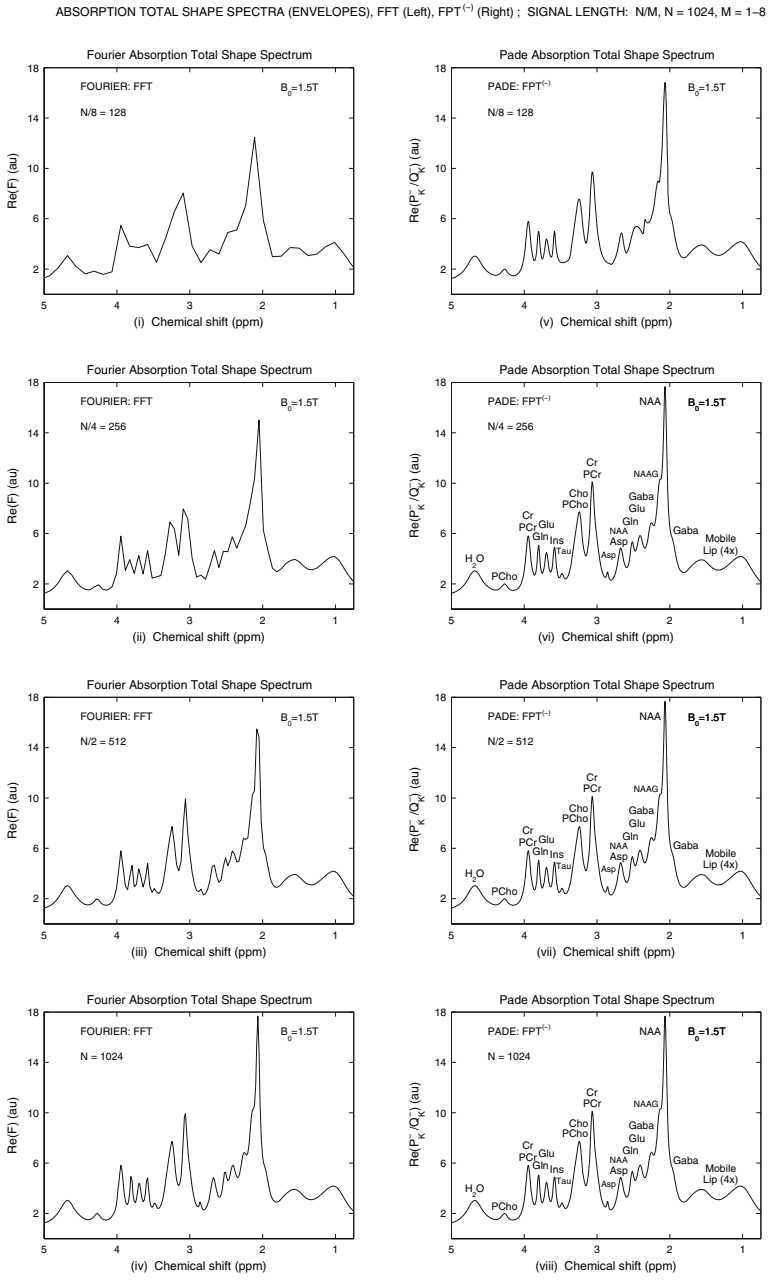

Fig. 3 Performance comparison of the fast Fourier transform (*left column*) and fast Padé transform (*right column*) at one eighth ($N/8 = 128$), one quarter ($N/4 = 256$), one half ($N/2 = 512$) and full ($N = 1024$) signal lengths. The acronyms for metabolite at the corresponding positions are on the *right panels*. Spectra correspond to an FID typically encoded clinically from a healthy human brain via MRS using an external static field $B_0 = 1.5\,T$ and a short TE of 20 ms, with total length $N = 1024$ and bandwidth 1000 Hz so that $t = 1$ ms (see e.g., [56]). Adapted from Ref. [50]

if the spectral parameters are obtained in a reliable way with an intrinsic and robust error analysis, accompanied by the ability to clearly identify and thereby separate noise from the physical signal. This is uniquely provided by the FPT via the powerful concept of noise filtering called the Froissart doublets (pole-zero cancellations) [51].

2 Theory

As elaborated in detail [35,37,50,51,59] the theoretical basis for the mathematical model for any time signal and the corresponding spectrum emerges *uniquely* from the quantum dynamics of the investigated system. This is because signal processing, which has thus far been considered as a discipline on its own, is part of a larger theoretical framework—the most successful physics theory: quantum mechanics. This determines that the optimal mathematical model for the frequency spectrum of time signals is prescribed quantum-mechanically to be the ratio of two polynomials, i.e., the FPT. Thus, just as in the time domain where quantum mechanics predicts the form of the time signal as the sum of complex-valued damped exponentials, by virtue to the time-frequency dual representation, the same physics automatically prescribes that the frequency spectrum is given by the Padé quotient of two polynomials. *This is the origin of the unprecedented algorithmic success of the FPT, via its demonstrable, exact reconstructions*, as shown in our Refs. [35,50,51].

The polynomial quotient P_K/Q_K (diagonal) or P_{K-1}/Q_K (para-diagonal) as a rational function in harmonic variable $z^{-1} = \exp(-i\omega\tau)$, is known in the literature as the Padé approximant (PA). In signal processing, the PA is alternatively called the fast Padé transform [64,65] to highlight the possibility of obtaining a shape spectrum from an FID via a non-parametric estimation as reminiscent of the FFT. The latter type of estimation in the FPT is done by simply evaluating the Padé spectrum P_K/Q_K without ever searching for any of the spectral parameters that are the complex frequencies $\{\omega_k\}$ and amplitudes $\{d_k\}$. The FPT is the only parametric estimator which computes the envelope spectrum without the need to obtain the set $\{\omega_k, d_k\}$ first. This is in sharp contrast to e.g., HLSVD [61], which computes the envelope spectrum by first estimating the peak parameters $\{\omega_k, d_k\}$. Most importantly, the FPT can perform parametric reconstructions by rooting the polynomial Q_K whose roots $\{z_k^{-1}\}$ yield $\{\omega_k\}$ and this readily leads to $\{d_k\}$ for each resonance. For example, the para-diagonal FPT treats the exact spectrum, i.e., the mentioned finite-rank Green function $G_N(z^{-1})$, via the *unique* ratio of two polynomials $P_{K-1}(z^{-1})/Q_K(z^{-1})$ at *any frequency* ω:

$$G_N(z^{-1}) = \frac{1}{N}\sum_{n=0}^{N-1} c_n z^{-n}, \tag{2}$$

$$G_N(z^{-1}) \approx \frac{P_{K-1}(z^{-1})}{Q_K(z^{-1})} = \sum_{k=1}^{K} \frac{d_k}{z^{-1} - z_k^{-1}}, \tag{3}$$

$$P_{K-1}(z^{-1}) = \sum_{r=0}^{K-1} p_r z^{-r}, \quad Q_K(z^{-1}) = \sum_{s=0}^{K} q_s z^{-s}, \tag{4}$$

where $z = e^{i\omega\tau}$ and $z_k = e^{i\omega_k\tau}$. The para-diagonal ($L = K-1$) and diagonal ($L = K$) PA are most frequently used from the set of the general PA, P_L/Q_K, because they incur minimal error in practice. In the FPT, the sum $\sum_{k=1}^{K} d_k/(z^{-1} - z_k^{-1})$ represents the complex-valued *total shape spectrum* (envelope) which is the sum of the K corresponding *component spectra*, $d_k/(z^{-1} - z_k^{-1})(1 \le k \le K)$. Here, P_{K-1} and Q_K are readily extracted from the input data G_N by treating the product $G_N Q_K$ in the defining relation $G_N * Q_K = P_{K-1}$ as the standard convolution [35,65,66].

3 Signal processing

We perform computations [35,49] using the FPT to reconstruct spectral parameters for an MRS time signal which closely matches FIDs encoded on clinical scanners via proton MRS from the brain of a healthy volunteer [55,56]. Using the FPT to analyze the FIDs, the coefficients $\{p_r, q_s\}$ of the polynomials P_{K-1} and Q_K are computed efficiently by solving the systems of linear equations deduced from definition (2). In so doing, we recognize that the product in $G_N(z^{-1}) * Q_K(z^{-1}) = P_{K-1}(z^{-1})$ is a convolution, as mentioned [65,66]. Once $\{p_r, q_s\}$ are obtained, the (non-parametric) envelope spectrum can be computed by evaluating the quotient $P_{K-1}(z^{-1})/Q_K(z^{-1})$ at any selected frequency ω, as stated. To extract the peak parameters, one solves the characteristic equation $Q_K(z^{-1}) = 0$. This polynomial equation has K unique roots $z_k^{-1}(1 \le k \le K)$, so that the sought ω_k is deduced via $\omega_k = (i/\tau)\ln(z_k^{-1})$. A similar procedure applies to the diagonal FPT. Peak assignments are made according to the most accurate available in vitro data from e.g., Refs. [25,31,67,68]. For reliable quantifications in MRS, it is not only the peak positions $\mathrm{Re}(\omega_k)$ that count[4]; the peak widths $\mathrm{Im}(\omega_k)$ and the complex amplitudes d_k are also critical. This is because the kth metabolite concentration is computed from the reconstructed peak parameters. From the spectral parameters, one can deduce the peak area underneath each resonance. Peak area is proportional to the concentration of the metabolite, relative to a selected reference concentration (water or another metabolite). Therefore, even for accurately determined ω_k's, the problem of obtaining the precise estimates of the d_k's becomes extremely important. In the FPT, the kth amplitude d_k depends only upon the kth root z_k^{-1} and it is obtained analytically from the Cauchy residue theorem [35,36,50]. Moreover, unlike guessing in HLSVD and in all the fitting algorithms from MRS, the FPT determines the true number K of resonances exactly, by e.g., the concept of Froissart doublets (pole-zero cancellations) [51,69]. Overall, the FPT completely avoids fitting and accomplishes accurate quantification by reliably extracting the parameters of all the physical metabolites directly from the raw, unedited, encoded FID. Specifically, when used as a parametric estimator, the FPT first explicitly finds all the peak parameters $\{\omega_k, d_k\}(1 \le k \le K)$ of every physical resonance *without ever using the Fourier spectrum*, or any other spectrum. A spectrum can be subsequently constructed for e.g., visualization purposes, in any of the desired modes (absorption, magnitude, dispersion, power).

[4] Hereafter, $\mathrm{Re}(u)$ and $\mathrm{Im}(u)$ denote the real and imaginary parts of a complex number u.

4 Results

4.1 Practical implementation of the benchmarked FPT for extracting metabolite concentrations from MRS signals

As presented in detail in [37], benchmark studies have now been performed demonstrating that the FPT provides the urgently needed accuracy in extracting metabolite concentrations from MRS signals.

The next step is the practical implementation of this methodology, so that it can become a hands-on tool for clinicians. In Fig. 4 an example is shown of how this can be achieved, from the analysis performed in Refs. [50,51,69]. This was for an MRS time signal that closely matches FIDs encoded via proton MRS from the brain of a healthy volunteer [56]. The parameters for each of the 25 reconstructed peaks are first presented in the upper left panel (i) of Fig. 4. These are the position, width and absolute value of the amplitude. Then, in the upper right panel (iv), the metabolite assignments are given. It is seen, e.g., that there are four mobile lipid components whose peaks ## 1–4 are in the frequency range between 0.985 and 1.689 ppm. The T_2 relaxation times and the numerical values of the concentrations for each of these 25 metabolites are given, computed using the width and amplitudes with the Larmor frequency of 63.864 MHz corresponding to the magnetic field strength of 1.5 T. In addition, the fraction of the concentration of a given metabolite is shown relative to that which is most abundant (in the present example this is peak #6 corresponding to NAA at 2.065 ppm). Thus, for example, it is seen that peak #16 corresponding to choline (Cho) at 3.239 ppm has a concentration of 6.240 mMol/ww and its ratio to NAA at 2.065 ppm is 0.56. The component spectrum is shown with the peak numbers in the left middle panel (ii) of Fig. 4 and the total shape spectrum on the right middle panel (v). Comparing these two middle panels, it is clear that many of the peaks are closely overlapping, and could not be deciphered with certainty from the total shape spectrum. In the bottom left panel (iii), the peak assignments together with the peak numbers are given for each of the 25 components, with the localization of the peaks. The absorption total shape spectrum (as the sum of all the absorption component shape spectra with all the peak assignments) is displayed on the bottom right panel (vi).

Especially instructive and rewarding for the spectral decomposition by the FPT is to compare the left and right bottom panels (iii) and (vi) in Fig. 4. There, we can clearly see how deceiving and misleading it is to attempt to surmise which components are hidden underneath a spectral structure. For example, rather than reconstructing exactly four mobile lipids under the two broad structures in the range 1–2 ppm, as done unambiguously by the FPT, equally acceptable (in the least-square sense) results of fitting by the customary methods from MRS (VAPRO, AMARES, LCModel, etc.) could "reconstruct" three, five or more peaks that would all give the same absorption total shape spectrum from 1 to 2 ppm, similarly to the Lanczos paradox [39,40]. Similar or even more serious problems with clinically unacceptable ambiguities stemming from fittings are found to occur in several other parts of the spectrum from panel (vi) of Fig. 4. For example, to use fitting to guess that the peaks close to 2.7 ppm are, in fact, nearly degenerate (each comprised to two components with exceedingly close chemical shifts differing from each other by 0.001 ppm) would be certainly impossible.

EXACT RECONSTRUCTION of SPECTRAL PARAMETERS, CONCENTRATIONS and ABSORPTION COMPONENT SPECTRA: FPT$^{(-)}$

Peak #	Position	Width	|Amplitude|
1	0.985	0.180	0.122
2	1.112	0.257	0.161
3	1.548	0.172	0.135
4	1.689	0.118	0.034
5	1.959	0.062	0.056
6	2.065	0.031	0.171
7	2.145	0.050	0.116
8	2.261	0.062	0.092
9	2.411	0.062	0.085
10	2.519	0.036	0.037
11	2.675	0.033	0.008
12	2.676	0.062	0.063
13	2.855	0.016	0.005
14	3.009	0.064	0.065
15	3.067	0.036	0.101
16	3.239	0.050	0.096
17	3.301	0.064	0.065
18	3.481	0.031	0.011
19	3.584	0.028	0.036
20	3.694	0.036	0.041
21	3.803	0.024	0.031
22	3.944	0.042	0.068
23	3.965	0.062	0.013
24	4.271	0.055	0.016
25	4.680	0.136	0.113

(i) N_P=256: Position (ppm), Width (ppm), |Amplitude| (au)

Peak #	Chem. Sh.	Relax.	Concentr.	Fraction	Assignm.
1	0.985	0.087	7.930	0.71	Mob. Lip
2	1.112	0.061	10.46	0.94	Mob. Lip
3	1.548	0.091	8.775	0.79	Mob. Lip
4	1.689	0.133	2.210	0.20	Mob. Lip
5	1.959	0.251	3.640	0.33	Gaba
6	2.065	0.501	11.12	1.00	NAA
7	2.145	0.313	7.540	0.68	NAAG
8	2.261	0.251	5.980	0.54	Gaba
9	2.411	0.251	5.525	0.50	Glu
10	2.519	0.435	2.405	0.22	Gln
11	2.675	0.477	0.520	0.05	Asp
12	2.676	0.251	4.095	0.37	NAA
13	2.855	0.971	0.325	0.03	Asp
14	3.009	0.245	4.225	0.38	Cr
15	3.067	0.435	6.565	0.59	PCr
16	3.239	0.313	6.240	0.56	Cho
17	3.301	0.245	4.225	0.38	PCho
18	3.481	0.504	0.715	0.06	Tau
19	3.584	0.555	2.340	0.21	m–Ins
20	3.694	0.431	2.665	0.24	Glu
21	3.803	0.655	2.015	0.18	Gln
22	3.944	0.377	4.420	0.40	Cr
23	3.965	0.251	0.845	0.08	PCr
24	4.271	0.285	1.040	0.09	PCho
25	4.680	0.115	7.345	0.66	Water

(iv) N_P=256: Chem. Sh. (ppm), Relax. T_2 (s), Conc. (mMol/ww)

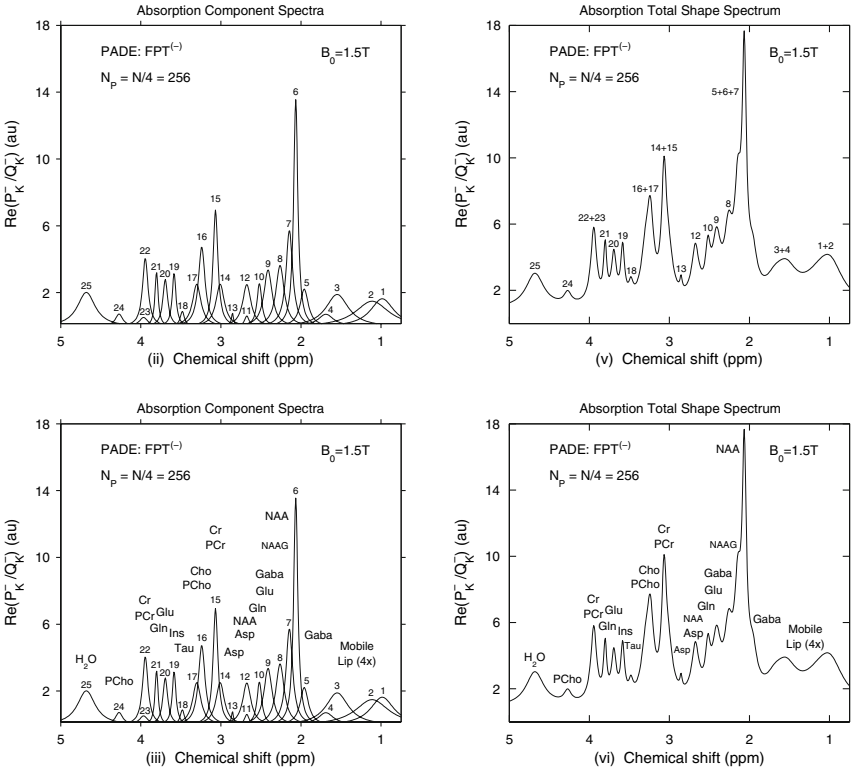

Fig. 4 Padé-reconstructed converged spectral parameters, metabolite concentrations and absorption component spectra corresponding to an FID typically encoded clinically from a healthy human brain via MRS using an external static field $B_0 = 1.5$ T and a short TE of 20 ms, with total length $N = 1024$ and bandwidth 1000 Hz so that $t = 1$ ms (see e.g., [56]). *Top panels* (i) and (iv): spectral parameters (*left*), assignments, T_2 relaxation times, concentrations and fraction of NAA at 2.065 ppm (*right*). The acronym ww denotes wet weight. *Middle panels* (ii) and (v): absorption component spectra with peak numbers (*left*), absorption total shape spectrum with peak numbers (*right*). *Bottom panels* (iii) and (vi): absorption component spectra with peak numbers and metabolite assignments (*left*), absorption total shape spectrum with metabolite assignments (*right*)

Figure 4 is deemed to be most helpful for clinicians, since it gives both a graphic and a quantitative overview of MRS. By enabling repeated cross-checking between these two presentations, the clinician will more easily acquire a deeper grasp of the method, together with acumen in interpretation of patterns typical of malignancy versus benign pathologies. This approach is illustrated later (see also [57,58]), with the spectral features, metabolite concentrations and assignments from MRS, comparing cancerous and benign ovarian cyst fluid. The benchmark studies described in [37], together with the practical implementation described here represent a valid, exact, and long awaited approach to quantification of MRS signals. Via this type of implementation, Padé-optimized MRS is set to indeed very soon become a standard diagnostic tool for oncology, and beyond.

4.2 Separation of spurious (non-physical) from genuine (physical) information for noiseless MRS data

The FPT has been shown to resolve and quantify tightly overlapped and even nearly degenerate resonances that are abundantly present in MR spectra generated using encoded in vivo time signals. Only within the FPT, pole-zero cancellation (Froissart doublets) can be used to unequivocally distinguish true from spurious resonances. This is demonstrated here in the noise-free case, but also for synthesized MR time signals corrupted by noise at a level similar to realistic encoding conditions for the full Nyquist range (from -3 to over 12 ppm), as presented in Ref. [37].

The number of spurious resonances is always several times greater than that of the true metabolites. It is obviously an essential precondition for trustworthy clinical applications that the genuine information be clearly and unambiguously identified. In recent studies [51,69] via the powerful concept of Froissart doublets (pole-zero cancellations), the FPT has been shown to achieve this task.

In Ref. [51], we have validated a powerful means of determining whether a given reconstructed resonance is true or spurious. This is done by computing a sequence of the Padé shape spectra $\{P_m/Q_m\}(m = 1, 2, 3, \ldots)$ in the frequency range of interest, say 0.5–5 ppm, as in Ref. [51]. Here, the fingerprint of detection of the exact number K of resonances is the attainment of the stabilization value $m = m'$ after which a saturation is systematically maintained by observing that $P_{m'+q}/Q_{m'+q} = P_{m'}/Q_{m'}(q = 1, 2, 3, \ldots)$. This critical transition $(m = m')$ yields the sought K via $K = m'$, as verified to work in practice with MRS signals [51]. This is the concept of Froissart doublets, or equivalently, pole-zero cancellations [50,51,69,70].

Specifically, the computation is carried out by gradually and systematically increasing the degree of the Padé polynomials. As these degrees change, the reconstructed spectra fluctuate until stabilization occurs. The value of the polynomial degree at which the predetermined level of accuracy is achieved represents the sought exact number of resonances K. This constancy of the reconstructed values can be obtained, e.g., via the cannonical representation of the Padé polynomial quotients:

$$\frac{P_{K-1}^{\pm}(z^{\pm 1})}{Q_K^{\pm}(z^{\pm 1})} = \frac{p_{K-1}^{\pm}}{q_K^{\pm}} \frac{\prod_{k=1}^{K-1}(z^{\pm 1} - \tilde{z}_k^{\pm})}{\prod_{k'=1}^{K}(z^{\pm 1} - z_{k'}^{\pm})}, \tag{5}$$

where $\tilde{z}_k^{\pm}$ and $z_k^{\pm}$ are the zeros of polynomials $P_{K-1}^{\pm}$ and $Q_K^{\pm}$, respectively. The quotient form from Eq. (2) leads to cancellation of all the terms in the Padé numerator and denominator polynomials, when the computation is continued after the stabilized value of the order in the FPT has been attained, so that:

$$\frac{P_{K-1+m}^{\pm}(z^{\pm 1})}{Q_{K+m}^{\pm}(z^{\pm 1})} = \frac{P_{K-1}^{\pm}(z^{\pm 1})}{Q_K^{\pm}(z^{\pm 1})}, \quad (m = 1, 2, 3, \ldots). \tag{6}$$

The Cauchy residue of $P_{K-1}^{\pm}/Q_K^{\pm}$ from Eq. (5) represents the amplitudes $d_k^{\pm}$ whose analytical expressions are:

$$d_k^{\pm} = \frac{p_{K-1}^{\pm}}{q_K^{\pm}} \frac{\prod_{k'=1}^{K-1}(z_k^{\pm 1} - \tilde{z}_{k'}^{\pm})}{\prod_{k'=1,k'\neq k}^{K}(z_k^{\pm 1} - z_{k'}^{\pm})}. \tag{7}$$

Therefore, it is obvious from Eq. (7) that whenever $z_k^{\pm} = \tilde{z}_k^{\pm}$, the amplitudes $d_k^{\pm}$ of the poles from the Froissart doublets are exactly zero:

$$d_k^{\pm} = 0 \quad \text{for} \quad z_k^{\pm} = \tilde{z}_k^{\pm}. \tag{8}$$

In Fig. 5, we illustrate the concept of Froissart doublets for the noiseless case of a synthesized FID derived from realistic MRS data encoded at 1.5 T (the same as was used in Ref. [37]). We use the diagonal form of the FPT with its convergence region inside the unit circle, namely FPT$^{(+)}$ [35,49]. After convergence has been reached, there is a total of 128 resonances, but only 25 of these are genuine. The remaining 103 are spurious resonances. These spurious resonances are generated, since we did not stop increasing the varying polynomial order m in the Padé quotient P_m^+/Q_m^+ until this latter ratio eventually reached its plateau or constancy region. Such a stabilized value of P_m^+/Q_m^+ was nowhere in sight at $m = 25$, which happens to be equal to the input number of resonances. In other words, once the synthesized FID has been sampled, we intentionally forget that we ever knew the true number of resonances and any of their spectral parameters. From that point on, we treat the synthesized FID as an input data of a totally unknown internal structure, just as if it were obtained in experimental encoding. The top panel of Fig. 5 shows that all these spurious resonances are Froissart doublets, namely that the poles stemming from the denominator polynomial, marked as open circles automatically coincide with the corresponding zeros of the numerator polynomial denoted by small filled circles (or dots). This is a graphic representation of pole-zero cancellation. In contrast, there are 25 tightly-packed genuine resonances. In the case of the FPT$^{(+)}$, all the imaginary parts of the genuine and spurious frequencies are positive and negative, respectively (see Fig. 5). Thereby, the genuine chemical shifts between 0.985 and 4.68 ppm are clearly separated from the spurious resonances.

In the bottom panel of Fig. 5, it can be seen that all the spurious resonances have amplitudes equal to zero, as per (8). At one-quarter of the total signal length ($N/4 = 256$) for the 25 true reconstructed resonances the absolute values of the amplitudes are all seen to have non-zero values. Moreover, these exactly coincide with the input data,

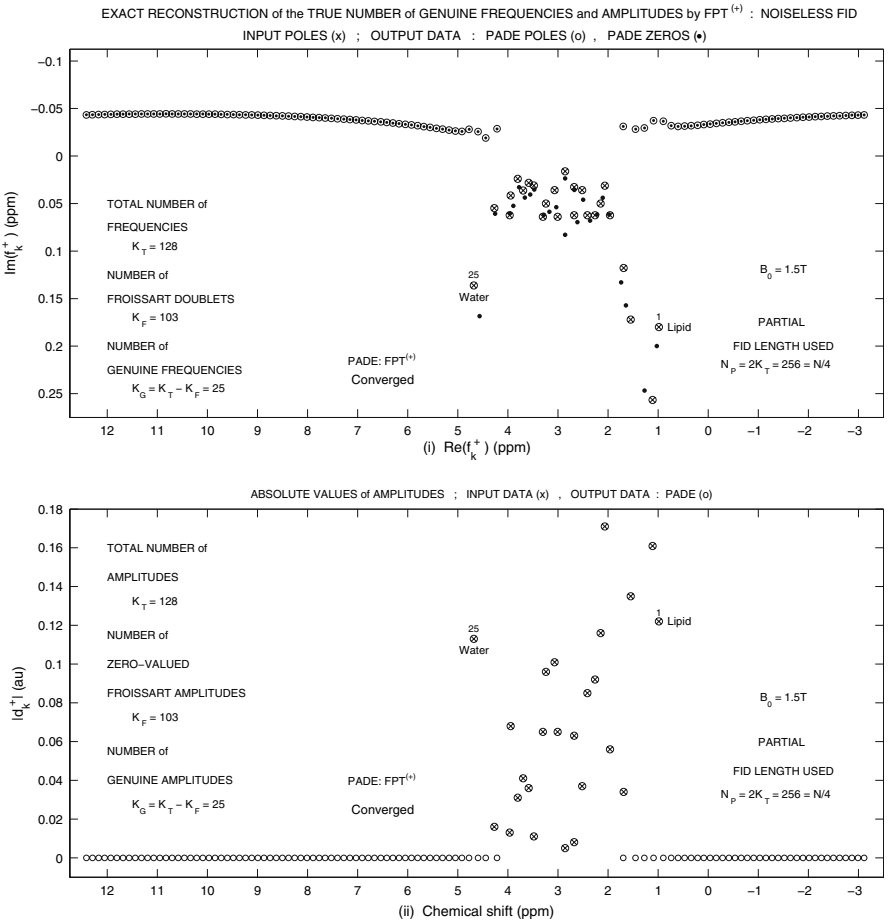

Fig. 5 *Top panel* (i): use of Froissart doublets to unequivocally extract the exact number K_G of genuine frequencies and amplitudes from the total number of the spectral parameters reconstructed by the FPT$^{(+)}$ for the noise-free time signal. The FPT$^{(+)}$ separates the genuine from spurious frequencies in the two non-overlapping regions, $\mathrm{Im}(f_k^+) > 0$ and $\mathrm{Im}(f_k^+) < 0$, respectively. *Bottom panel* (ii): all the spurious (Froissart) amplitudes are identified by their zero values. Adapted from Ref. [51]

since full convergence has been achieved at this signal length. Again, the spurious resonances appear in all the parametric estimators that must use more than twice the number of unknown frequencies and amplitudes. This leads to an over-determined system which yields more resonances than the actual number present in the analyzed signal. The extra resonances are spurious and act as "noise" or are "noise-like", even in the case of a noiseless signal. The problem is first to identify these and then discard them. Among all the estimators, only the FPT can achieve this task with certainty, and this is done through the concept of the Froissart doublets, which acts as a powerful filter of spurious "noise-like" resonances, as illustrated in Fig. 5.

Distinction of genuine from spurious peaks has been one of the thorniest challenges to MRS. Solving this problem is of urgent clinical importance, particularly for can-

cer diagnostics. For application of the Froissart filter to noise-corrupted synthesized FIDs, see Ref. [37]. Needless to say, these noisy time signals are truly reminiscent of experimentally measured FIDs.

4.3 Relevance of the FPT for direct application to MRS data from oncology

4.3.1 Distinction of malignant from benign ovarian lesions: exact calculation of metabolite concentrations via MRS

In Refs. [57] and [58], the FPT was applied for the first time to MRS signals from malignant and benign ovarian lesions. This problem area was chosen because of its urgent clinical importance, namely that early ovarian cancer detection would have a major survival benefit, and that the currently available methods have low diagnostic accuracy. As mentioned, because of the small size and motion of this organ, in vivo MRS is mired by problems of resolution and SNR, and yet, there is a rich store of MR-observable compounds that distinguishes benign from cancerous adnexal masses when in vitro MRS is applied. We postulate that Padé-optimized MRS could help overcome the current problems hindering the acquisition of high quality MR data from the ovary, and thereby enable in vivo MRS to become the method of choice for detecting cancerous adnexal lesions.

Having applied the FPT to data derived from benign and malignant ovarian cyst fluid encoded at high magnetic fields $B_0 = 14.1$ T in vitro [31], we have obtained numerical results as presented Refs. [37,57,58]. We have also specifically examined the convergence pattern of the concentrations of the metabolites for benign versus malignant ovarian cyst fluid. In Fig. 6, the chemical shifts are presented along the abscissae of the six panels (i)–(vi), with concentrations as the ordinates. The input data are represented by the symbol x, whereas the Padé-reconstructed data are shown as open circles. The data corresponding to the benign and malignant cases are presented in the left [(i)–(iii)] and right panels [(iv)–(vi)], respectively. Prior to convergence, at $N/32 = 32$ [top panels (i) and (iv)], the only metabolite for which the correct concentrations were obtained in both the benign and malignant cases is glucose at 5.22 ppm [1387 μ mol/L (benign) and 260 μ mol/L (malignant), respectively]. At $N/16 = 64$ [middle panels (ii) and (v)] and $N/8 = 128$ [bottom panels (iii) and (vi)], all of the reconstructed metabolite concentrations are correct, as seen both numerically and by the graphic representations. For $N/16$ and $N/8$, this means that the x's are completely centered within the open circles, indicating full agreement between the input and reconstructed data. Figure 7 recapitulates the absorption spectra and the retrieved concentrations with the full convergence achieved by the FPT using only 64 FID points out of 1024 data sampled in the time domain. This combined plot illustrates the overall power of the FPT which performs shape estimation and quantification on the same footing without any post-processing and with no reliance upon other estimators.

Figure 7 is deemed to be most helpful for clinicians, since it gives both a graphic and a quantitative overview of the inner working of MRS. Specifically, such a procedure as depicted on this figure, represents a comprehensive summary of signal processing, encompassing line-shape estimation *and* quantification, which culminates in the

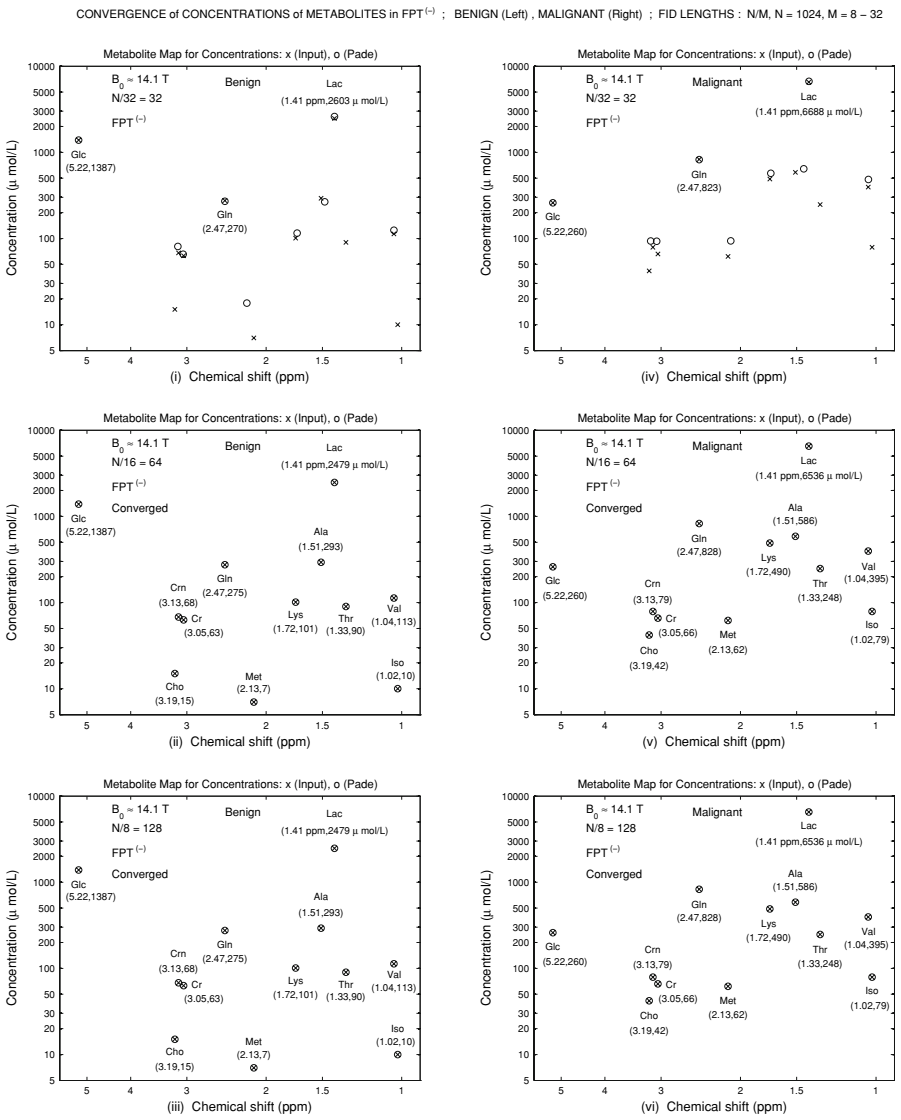

Fig. 6 Convergence of the Padé-reconstructed concentrations of the metabolites for the benign (*left column*) and malignant (*right column*) ovarian cyst data from [31]. At $N/32 = 32$, convergence has not yet been achieved [*top panels* (i) and (iv)], whereas at $N/16 = 64$, the reconstructed concentrations for all the 12 metabolites have converged [*middle panels* (ii) and (v)]. This convergence is stable, at longer signal lengths, as shown in *bottom panels* (iii) and (vi) at $N/8 = 128$ signal points, and it remains so, as we have explicitly checked, at $N/4 = 256$, $N/2 = 512$ and $N = 1024$. Adapted from Ref. [57]

reconstructed concentrations as the diagnostically most relevant information from the examined tissue.

Recent papers [57,58] were based upon the median values obtained for the metabolite concentrations estimated from the experimental data encoded by Boss et al.

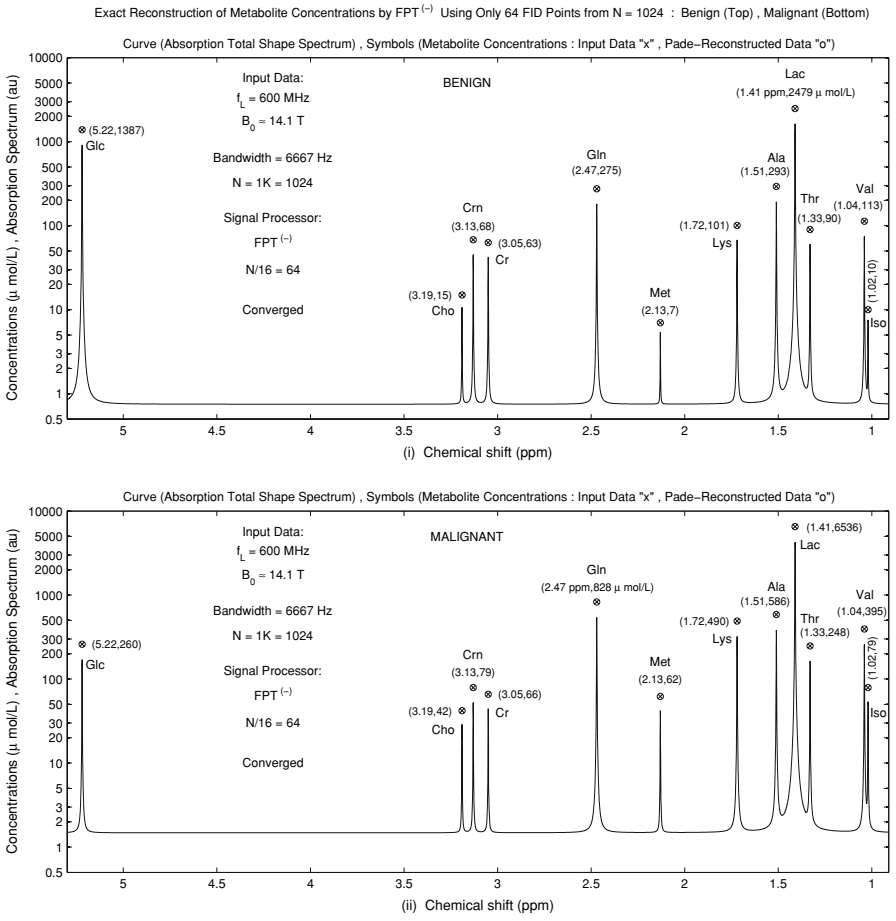

Fig. 7 Absorption spectra at full convergence ($N/16=64$) achieved by the FPT for the benign [*top panel* (i)] and malignant [*bottom panel* (ii)] ovarian cyst fluid FIDs derived from the corresponding experimentally measured time signals [31], with the retrieved concentrations of the 12 metabolites indicated above the corresponding peak. Adapted from Ref. [57]

[31]. Studies [57] and [58] use noise-free FIDs, since we wanted to set up the fully-controlled standard for the FPT in the case of the initial application of this method to data within the realm of ovarian cancer diagnostics by MRS. This is methodologically justified [50]. We are currently extending our analysis to noise-corrupted synthesized data (still well-controlled) and to encoded FIDs. We are also including *doublet and multiplet resonances*, since they are present in the encoding [31], as well.

As stated, the high resolution of the FPT could also be of benefit for in vivo MRS investigations, for which, poor SNR has been a major obstacle which hampered progress in ovarian cancer diagnostics via MRS. It has been suggested that in vivo MRS could become the method of choice for accurate detection of early stage ovarian cancer, insofar as the current obstacles hindering the acquisition of high quality time signals

and the subsequent reliable analysis of spectra as well as their interpretation can be surmounted [32].

Therefore, we plan as the next step to apply the FPT in a combined study of malignant versus benign ovarian lesions, in which in vitro and in vivo clinical correlations together with histopathology can be provided for cross-verification. This type of image-histopathology correlation is considered to be particularly promising for improving the diagnostic accuracy of MRS and MRSI in oncology [71]. Moreover, MRS and particularly MRSI with its advantageous full volumetric coverage can provide additional, complementary information which in some cases can even enhance the accuracy of histopathology [71]. Thus, Mountford et al. [72] state that MRS is "now poised to be introduced into the pathology laboratory as an adjunct to, and in some cases replacement for difficult pathologies. . . the combination of MRI and MRS in vivo with correlative MRS on biopsy currently offers an unprecedented accuracy for the diagnosis and prognosis for human diseases" (p. 3701).

4.3.2 The FPT applied to MRS data derived from breast cancer tissue, fibroadenoma and normal breast tissue

The FPT is now being applied for the first time to MRS data from breast cancer, fibroadenoma and normal breast tissue. We chose this problem area because of its clinical urgency and also to continue our earlier studies. Our previous examination via detailed paired and logistic regression analysis [23,24,73] confirmed a very rich opportunity for information extraction provided by in vitro ^{1}H MRS analysis of metabolite concentrations in malignant versus non-cancerous breast tissue [25]. Several metabolites (most notably lactate, which yielded 100% correct predictions) showed promise with respect to diagnostic accuracy. Elevated lactate reflects the presence of cancer cells whose energy source comes from the anaerobic glycolytic pathway. Animal models of breast cancer also support the importance of assessing the rate of glycolysis and lactate clearance with respect to the diagnosis and prognosis of breast cancer. Thus far, however, in vivo ^{1}H MRS has not included lactate as a metabolic marker of breast cancer. In vitro data also reveal that breast cancer samples are associated with a significantly higher phosphocholine (PCho) to glycerophosphocholine (GPC) ratio compared to the normal, non-infiltrated tissue [74]. These findings corroborate human breast cell line research, indicating that malignant transformation is associated with a so-called "glycerophosphocholine to phosphocholine switch" [74], which is related, *inter alia*, to over-expression of the enzyme choline kinase responsible for PCho synthesis, and also reflecting altered membrane choline phospholipid metabolism [75,76]. The three proton MR visible choline compounds are choline (3.21 ppm), PCho (3.22 ppm) and GPC (3.23 ppm), underscoring the clinico-biological importance of analyzing the relationship among these very closely overlapping resonances [73]. On the other hand, by summing these three metabolites as "total choline", as is currently done with in vivo MRS, differential information about the component metabolites for breast cancer diagnostics is irretrievably lost.

Our current work applying the FPT to MR data derived from normal and malignant breast tissue, as well as fibroadenoma [25] is being carried out with a similar approach

to what we have used previously on the subject of ovarian cancer [57,58]. Along these lines, the initial results [77] suggest that the FPT provides clear delineation and quantification of diagnostically important metabolites such as lactate which overlaps with lipid, as well as choline, phosphocholine and glycerophosphocholine that are closely overlapping to within 0.01 ppm. Moreover, the resolution performance of the FPT is markedly superior to that of the conventional Fourier-based analysis with respect to MR data from the breast.

As noted, breast cancer diagnostics using in vivo MRS have relied mainly upon assessments of the composite choline peak. Notwithstanding the need to expand the number of metabolites upon which this diagnosis is made, accurate quantification of total choline via the FPT would represent a major breakthrough both for early detection of breast cancer and for assessment of response to therapy [11,19,26]. One of the main current problems with attempts at quantifying total choline has been subjectivity due to the uncertainty with lower and upper integration limits when using the procedure of numerical quadratures to determine the concentration via peak integration, as typically done [31]. As mentioned, this problem does not occur with the FPT, since this processor yields the spectral parameters unequivocally, thereby obviating any subjective assessment about where a given peak begins and ends.

Moreover, the improved resolution and SNR provided by the FPT could help detect low concentrations of total choline and its components. Furthermore, the FPT could offer the possibility of detecting potentially informative resonances with short T_2 relaxation times, that will have decayed at longer TE, such as myoinositol, whose concentration yielded the clearest distinction between breast cancer and fibroadenoma in our analysis [23,24,73] of in vitro MRS data from Ref. [25], as mentioned.

The FPT will also be used for quantitative analysis of MR signals from non-malignant lesions that have thus far presented differential diagnostic dilemmas, notably benign tumors, infectious or inflammatory lesions. It will be particularly important to consider benign breast conditions that are difficult to distinguish from breast cancer using other non-invasive diagnostic modalities. These challenging differential diagnoses include e.g., ductal hyperplasia, fibroadenoma and fibrocystic changes. The normal lactating breast also has high concentrations of choline.

Poor specificity is currently the major drawback of MR-based modalities with respect to breast cancer screening. For example, despite excellent spatial resolution and generally superior sensitivity for breast cancer, MRI has lower specificity than mammography [26,78,79]. Intensive surveillance programs with a large number of false positive findings may impact unfavorably upon quality of life. Thus, questions remain about the full appropriateness of breast MRI as a screening tool in asymptomatic, high-risk patients, with the need to improve specificity particularly underscored [24,80]. The potential of MRS to improve the specificity of MRI in early breast cancer detection has been underscored [26]. This was most recently illustrated in a series of 32 patients with non-contrast enhancing breast lesions, MRS would have reduced the number of biopsies by 68% on suspicious, but actually benign lesions, while not missing any of the breast cancers [81]. Insofar as the expected improvements in diagnostic accuracy are achieved by Padé-based in vivo MRS, this could then be applied in younger women at high risk for breast cancer with the aim of determining the suitability of this newly emerging methodology for screening/surveillance.

4.3.3 The FPT applied to MRS data derived from prostate cancer tissue, healthy glandular and stromal prostate tissue

Spectroscopic imaging through in vivo MRSI has made a major impact in prostate cancer, where this method provides diagnostic clarity unmatched by literally any other non-invasive approach. Compared to MRI alone, MRSI substantially improves the accuracy with which prostatic tumor and extracapsular extension are detected, as well as helping to distinguish cancerous prostate from benign prostatic hypertrophy [82]. Guidance as to the optimal site for biopsy has been substantially improved by MRSI. Other areas of clinical decision-making with respect to prostate cancer have also been impacted by MRSI. These include e.g., selection of treatment modality and timing, treatment planning with brachytherapy, and assessing tumour regression versus recurrence after treatment.

The ratio between two MR-observable metabolites, choline at 3.2 ppm and citrate (2.62–2.68 ppm), has been the cornerstone of applications of in vivo MRSI for prostate cancer detection. Citrate is generally used as an indicator of healthy secretory activity of prostate epithelial cells, while choline reflects phospholipid metabolism of cell membranes, and is a marker for membrane damage, cellular proliferation and density typical of malignant processes.

However, as noted, there are clinically important exceptions with respect to these two metabolites. For example, in stromal prostate tissue or metabolic atrophy, citrate levels are low without cancer being present. With benign prostatic hypertrophy (BPH) citrate can still be high despite coexistent malignancy. Overall, it has been noted that citrate and choline alone are not sufficiently accurate markers for distinguishing between various patterns of prostatic disease.

In vitro MRS reveals other metabolites whose levels help identify prostate cancer; these include: spermine, spermidine, polyamines, lysine, myoinositol, scylloinositol and taurine, etc. [68]. The first three of these are assigned to 3.1 ppm and lie therefore very close to choline at 3.2 ppm. Myoinositol has a short T_2 relaxation time and, hence, will have decayed at longer TE.

In an approach similar to Refs. [57,58], we are also currently applying the FPT for the first time to MR data derived from prostate cancer, healthy stromal and healthy glandular tissue, as encoded in Ref. [83]. Our initial results suggest that the FPT reliably retrieves the input parameters of spermine, spermidine, and choline, phosphocholine and glycerophosphocholine which are quite closely overlapping as well as other diagnostically important metabolites, and thereby provides the most accurate quantification. These analyses also include doublet and multiplet resonances, which are characteristic of several of the metabolites of importance for detecting prostate cancer [83], and represent another methodologic challenge for diagnostics.

Improved resolution and SNR are likewise clinically important for enhancing the diagnostic yield of MRS in detecting the presence and extent of abnormal metabolite levels in patients with prostate cancer [84]. Our initial results indicate that the Padé-optimized MRS will provide the needed resolution and SNR enhancement so that healthy, hypertrophic and malignant prostate tissue are better distinguished, compared to what current clinical practice has heretofore offered.

4.3.4 The FPT applied to MRS data derived from melanoma metastases in regional lymph nodes versus uninvolved nodes

As noted earlier, spectroscopic information from fine needle aspiration of biopsy specimens has been found to provide rapid and quite accurate detection of metastatic melanoma in lymph nodes [22]. The ratio of the area underneath the resonances in the region from 1.8 to 2.5 ppm (containing lipid, lactate and other metabolites) to that of choline-containing resonances in the region 3.1–3.3 ppm has been found to be significantly higher in excised benign lymph nodes compared to those containing melanoma [85]. It was thereby suggested that techniques such as in vivo proton MRS hold great promise for assessment of sentinel nodes in patients with melanoma [86]. However, in the more recent Ref. [22], diagnostic accuracy was still not sufficient, since it was based upon the pattern-recognition method. There were 7% so-called "fuzzy" samples both in the primary (56 melanoma and 62 benign samples) and in the secondary data sets (24 melanoma and 38 benign samples) that were excluded from the analysis. Among the remaining so-called "crisp" samples, sensitivity was 92.3 and 87.5% and specificity 90.3 and 90.3% in the primary and secondary data sets, respectively. However, customary data analysis of the FIDs was performed using the FFT with all its highlighted limitations.

Further, using the methodology of Refs. [57,58] on ovarian cancer, we are also applying the FPT to data derived from Ref. [22] of MR spectra from regional lymph nodes containing metastatic melanoma and from benign nodes. Of particular note is that there are several closely lying resonances such as creatine, phosphocreatine and lysine at 3.0 ppm that may yield further insights with quantification by the FPT, and may thereby improve the accuracy with which lymph nodes with melanoma metastases are distinguished from uninvolved nodes. These and other lymph nodes have also been listed in Ref. [71] as being among the areas where the diagnostic power of MRS could be invaluable.

We envisage thereafter, to apply the FPT in a combined study of malignant versus benign dermatologic lesions, in which in vitro and in vivo clinical correlations together with histopathology are provided for cross-verification. Particular attention will be paid to difficult differential diagnoses and precursor lesions such as dysplastic nevi. As noted, this type of image-histopathology correlation is considered to be particularly promising for improving the diagnostic accuracy of MRS and MRSI in oncology [71]. Moreover, MRSI with its advantageous full volumetric coverage can provide additional, complementary information which in some cases, as already mentioned, can even enhance the accuracy of histopathology [72] and, especially, can help define the extent of malignant disease.

From a practical viewpoint, it would be invaluable to connect an MRS scanner with an interface which would provide clinicians with readily interpretable spectral information from the investigated lesions. Such information would be displayed in a clinically optimal way through spectra for benign versus malignant lesions containing a quantitative review of the situation through metabolite concentration maps compared against the corresponding standards, when these become available (they are absent at present). This avenue has already been envisaged here and the appropriate illustrations for direct use by clinicians have been given on Figs. 4 and 7, respectively, for normal

brain and for ovarian cancer diagnostics. Clearly, a similar procedure would also apply to skin cancers and, in particular, melanomas.

It should also be emphasized that invasive cutaneous melanoma has shown a dramatic risk in both incidence and mortality, especially in the Nordic countries where there is a large fair-skinned Caucasian population. Other, albeit less dangerous forms of skin cancer, such as squamous cell and basal cell carcinomas are also increasing in Northern Europe and worldwide, and therefore represent an important, universal public health problem. Early detection and accurate differential diagnosis could potentially benefit from non-invasive methods such as Padé-optimized in vivo MRS.

4.4 Other aspects of optimization within MR

4.4.1 The fast Padé transform applied to customary MRI with single coils

For MRI, image artefacts with edge distortions occur due to truncation within the FFT, which cannot supply images that are simultaneously bright and sharp. This is because sharpness of images stems from improved resolution which in the FFT is obtained by increasing the number of grid points per axis. However, larger data sets unavoidably contain more noise, which, in turn, reduces brightness significantly. The performance of the FPT was assessed in [33] for multiple numerical integration (quadratures) that are commonly encountered in MR physics. Therein, it was demonstrated that the FPT greatly accelerates convergence (with increasing number of sampling points) and yields unprecedented accuracy within *12 decimal places* using only $N = 512$ or 1024 points relative to only *2 decimals* in the FFT [33]. Combined with its robustness and stability, it was expected in [33] that the FPT would emerge as the method of choice for MRI which is a two-dimensional (2D) quadrature. This indeed turned out to be the case later on [51]. In the meantime, we have implemented the 2D FPT for MRI [87]. We have found that the optimal resolution (sharpness) of the FFT (512×512) can also be achieved by the FPT using only 1/2 of the data record 512×512. This achievement of the FPT has less noise and, as such, exhibits the optimal brightness, as actually the FFT for the 512×512 data has, but without the needed sharpness. Hence, *the FPT can achieve simultaneous brightness and sharpness of images* [87]. This is opposed to the FFT, where image artefacts due to truncation errors render the two requisites about simultaneous brightness and sharpness mutually incompatible. Within the FFT which has no extrapolation features, truncation errors are unavoidable because of the impossibility to encode infinitely long data records.

4.4.2 The FPT applied to two-dimensional magnetic resonance spectroscopy

Two-dimensional MRS is customarily used to enhance detection of breast cancer [88] and ovarian cancer [31]. The advantage of 2D MRS is improved separation of overlapping resonances using cross-correlation plots. There is a very important and fundamental difference between 2D FFT and 2D FPT. Namely, the 2D FFT is a train of two one-dimensional (1D) FFTs applied sequentially, which amounts to the absence

of coherence. In contrast, the 2D FPT treats both axes simultaneously and on the same footing, thus enabling full access to extraction of all the coherence effects.

We have applied the FPT for the first time to 2D MRS signals. Our initial results [89] reveal marked improvement in resolution, relative to the customary approach using the FFT to these two-dimensional signals. In 2D MRS one of the time axes is usually long, but the other must be short to maintain reasonable scanning time. This is where estimators that can extract information from short time signals become indispensable. We have compared the FFT and FPT applied to a brain phantom using 2D FIDs, kindly provided by Dr. Albert Thomas from the Department of Radiology, University of California, Los Angeles, who encoded the data on a 1.5 T MRI scanner.

The computed 2D spectra were at the signal lengths $N_1 = 256$ and $N_2 = 1024$, with the resolution improvement clearly demonstrated in the FPT compared to the FFT. Moreover, the 2D FPT, $P_{K-1}(\omega_1, \omega_2)/Q_K(\omega_1, \omega_2)$, can perform quantification by rooting the bivariate denominator polynomial $Q_K(\omega_1, \omega_2)$ where the angular (ω_p) and linear (f_p) frequencies are related by $\omega_p = 2\pi f_p (p = 1, 2)$, as usual.

Thus, the FPT has been shown to fulfill this critical task of quantification in 2D MRS, which is virtually unfeasible by attempts to extend any of the available 1D fitting algorithms, such as the LCModel [44] etc., to 2D MRS. Various applications of the fast Padé transform to 2D MRS signals from malignant and benign breast and ovarian lesions are underway and will be reported in the near future.

4.4.3 Magnetic resonance spectroscopic imaging

As noted, molecular imaging can be accomplished by synergistically combining MRI and MRS to yield MRSI. Rather than selecting a single voxel from three orthogonal slices to encompass a specific volume, as is done in MRS, a spectrum in MRSI is obtained at each point of selected grids that can be of various sizes. Thereby, full volumetric coverage can potentially be achieved by MRSI. The advantages of MRSI for cancer diagnostics, relative to reliance upon single voxel techniques, have been repeatedly emphasized [16,52]. In particular, a single voxel of tissue pre-selected via MRS might not be sufficiently representative of the pathologic process of concern. On the other hand, MRSI through its multi-voxel coverage can help assess the degree of involvement of tumour with surrounding healthy tissue [16].

Since the time signals from MRSI are precisely of the same FID nature as those from MRS, clearly the FPT can also be applied with equal success to MRSI. We have performed initial applications of the FPT to MRSI and demonstrated improvements in the resolution of MRSI and mitigation of Gibbs phenomena [90].

Application of Padé-optimized MRSI will be of particular interest for improved target definition in radiation therapy (RT). Three-dimensional maps of metabolite ratios provided by MRSI are currently being used to optimally shape the margins for definition of prostate cancers and brain tumors, including glioblastoma multiforme, replacing the current definition of uniform margins [12,91]. This is particularly important for confident sparing of non-involved brain tissue. It is anticipated that with Padé-optimization of MRSI by providing maps of precise quantitative information about metabolites concentrations, this goal will be achieved with greater fidelity.

5 Relevance of the advantages of the fast Padé transform to diagnostics by magnetic resonance spectroscopy in clinical oncology

As presently expounded, magnetic resonance spectroscopy and spectroscopic imaging are increasingly recognized as potentially key diagnostic modalities in oncology. It is, therefore, urgent to overcome the shortcomings of current applications of MRS and MRSI in cancer diagnostics. We have explained why more advanced signal processing methods are needed, and have demonstrated that the fast Padé transform is the signal processing method of choice to achieve this goal. The unprecedented algorithmic success of the FPT emerges from the fundamental principles that link signal processing to the larger and most successful theory, which is quantum physics. Thus far, poor resolution has been a major obstacle to wider application of MRS and MRSI in oncology. The superior resolution capacity together with the stability of the FPT for MRS signals have been clearly established [35,36,47,58,64]. Benchmark studies have been performed in which the FPT is shown to provide exact quantification of MRS signals and thereby metabolite concentrations are reliably and unequivocally obtained with an intrinsic and robust error analysis [49,51,54,60,69].

Distinction of genuine from spurious (noisy and noise-like) resonances has been one of the thorniest challenges to MRS and MRSI. In practice, the number of spurious resonances is always several times larger than the true ones. It is obviously an essential prerequisite for trustworthy clinical applications that the genuine information be clearly identified. In our most recent papers, via the powerful concept of Froissart doublets, the FPT is shown to achieve this task, as well, by filtering out completely and with certainty all the spurious information from the final output data [51,69]. This new approach is given the name: "Signal–Noise Separation" with the acronym SNS. Thus, for the first time it is now possible to reconstruct the entire clinically relevant information about metabolites, including their concentrations, as the most critical data, without guessing about the veracity of this information, thus obviating the current need for fitting with its attendant ambiguities, the most notorious one being non-uniqueness of the attempted parametric estimation by VARPRO, AMARES, LCModel and other similar recipes.

We have directly applied the FPT to MRS data derived from malignant and benign samples from the ovary [57,58]. Padé-optimization is shown to provide dramatic improvement in resolution and yields the unequivocal, exact parametric data needed to reconstruct the metabolite concentrations that characterize ovarian cancer and distinguish this from non-malignant samples. This line of investigation is thus a promising avenue for improved early ovarian cancer diagnosis, which we intend to pursue intensively, given its urgent clinical importance and public health ramifications. Namely, early ovarian cancer detection would have a major survival benefit, and the currently available methods have low diagnostic accuracy (mainly due to poor specificity).

Currently, we are applying Padé-optimization to MRS data derived from breast, melanoma and prostate cancer, and initial results are also encouraging. Other applications of the FPT to MRI, 2D MRS and MRSI are expected to yield further improvements in various aspects of cancer diagnostics, including target definition for radiotherapy and assessment of response to therapy.

We anticipate that MRS via Padé processing will reduce the false positive rates of MR-based modalities and further improve the sensitivity of these methods. Once this is achieved, and given that MR-based diagnostic methods are free from ionizing radiation, new possibilities for cancer screening and early detection will open up, especially for risk groups, e.g., the application of Padé-optimized MRS in younger women at high risk for breast and/or ovarian cancer. The need for accurate quantification of closely overlapping resonances has been particularly underscored for breast cancer diagnostics using MRS.

Further, MRS with the accompanying Padé quantification applied to prostate cancer is particularly important for diagnostic enhancement, because of the current dilemmas surrounding prostate cancer screening (e.g., cutpoints of prostate specific antigen—PSA, etc.), as well as the public health importance of this malignancy.

There is a great need for a non-invasive diagnostic support for physicians in the early detection of malignant melanomas. A person may have up to 100 moles; distinguishing malignant melanomas from benign nevi is very difficult even for an experienced dermatologist. For a general practitioner, it is often an impossible task. Padé-optimized MRS seems to be an excellent candidate for further studies in this field by ultimately providing quantitative standards to better differentiate malignant melanomas from benign lesions.

It is fascinating that thus far MRS has made gigantic strides across several branches of medicine by relying merely upon a handful of metabolites or their ratios, or even only a single metabolite, such as total choline in the case of breast cancer. This restricted metabolite window stems directly from the limitations of the conventional data analysis based upon the fast Fourier transform and the accompanying post-processing via fitting and other related *phenomenological* approaches. It is, therefore, expected that the diagnostic yield and overall performance of MRS in oncology will be significantly enhanced by extracting reliable clinical information about many more metabolites. Precisely this considerable enlargement is currently facilitated by the fast Padé transform, on the basis of its proven validity, guaranteed by *the first principles* of physics and chemistry. As a research field and a clinical diagnostic modality, MRS is nowadays undergoing a veritable renaissance. Starting from its enviable status of a highly appreciated and well-established NMR method of analytical chemistry in research laboratories, MRS developed to such a point in medicine that it is currently being viewed by experts as the diagnostic modality which will possibly revolutionize not only diagnostics, but also guided surgery and target delineation for radiotherapy.

Working primarily within MRS applied to diagnostics in clinical oncology, we have systematically chosen to focus on the problems of critical and major public health concern, such as breast, prostate, melanoma and ovarian cancer, as well as brain tumors. We are doing this because we initially believed, and subsequently demonstrated, that we can further the much need progress in fighting these major diseases. Consensus exists worldwide among expert oncologists, that this fight must be a comprehensive strategy, including multi- and inter-disciplinarity with the strongest link to basic science research. The needed work in this area of biomedical signal processing for oncology, ultimately depends upon: (i) a deep knowledge of the origin and mechanism of generation of in vivo signals (ii) their clinical interpretation and identification of their informational content with a particular disease, and (iii) application of the extracted

information for clinical practice. Synergistically, many experts from different research disciplines are needed to cover the workable chain: clinical problem-underlying physiology-interpretation-clinical application with the aim of enabling Padé-based MRS to soon become a standard tool for clinical oncology. We have shown that Padé-based MRS, or MRS-FPT as it could justifiably be termed, is optimal to achieve this task because of its multifaceted advantages, encompassing theoretical, mathematical, strategic and, most importantly with respect to the presently highlighted applications, clinical aspects.

6 Conclusion

Accuracy, resolving power, convergence rate and robustness of any signal processor depend on such obvious input parameters as the signal-to-noise ratio, the SNR, and the total acquisition time of the investigated signal, or equivalently, the signal length for a given bandwidth. However, a number of more subtle features of spectral analysis play a decisive role of the overall performance capability of a given estimator. These include the configurations of the poles and zeros in the complex plane, their density in the selected part of the Nyquist range, the smallest distance among poles on the one hand and zeros on the other, inter-separations among poles and zeros, their distance from the real frequency axis, the smallest imaginary frequencies (the largest lifetimes of resonant states) in the spectrum, etc. Among the most suitable mathematical tools for investigation of the effects of the enumerated features are the Argand plots which show the imaginary part as a function of the corresponding real part of a given complex-valued quantities, such as the harmonic variables, the fundamental frequencies and the corresponding amplitudes. The present study has a focus on signal–noise separation, the SNS, which can be best illustrated by displaying the Froissart doublets in the Argand plots for complex fundamental frequencies.

Convergence in the fast Padé transform, the FPT, is achieved through stabilization or constancy of the reconstructed frequencies and amplitudes. Moreover, the accomplished stabilization is a veritable signature of the exact number of resonances. With any further increase of the partial signal length towards the full signal length, i.e., passing the stage at which full convergence has been reached, it is found that all the fundamental frequencies remain constant. Moreover, machine accuracy is achieved by the FPT, proving that when this signal processor is nearing convergence, it approaches straight towards the exact result with an exponential convergence rate (the spectral convergence). This proves that the FPT is an exponentially accurate approximation for functions customarily encountered in spectral analysis in MRS and beyond. The mechanism by which this is achieved, i.e., the mechanism which secures the maintenance of stability of all the spectral parameters, as well as constancy of the estimate for the true number of resonances is provided by the so-called pole-zero cancellation, or equivalently, the Froissart doublets. This signifies that all the additional poles and zeros of the Padé spectrum (given by the unique ratio of two polynomials), i.e., those beyond the stabilized number of resonances, will cancel each other. In other words, the FPT is safe-guarded against the contamination of the final results from extraneous resonances, since each pole due to spurious resonances stemming from the denominator

polynomial will automatically coincide with the corresponding zero of the numerator polynomial, thus leading to the pole-zero cancellation in the polynomial quotient of the FPT. Such pole-zero cancellations can be advantageously exploited to differentiate between spurious and genuine content of the signal. Since these unphysical poles and zeros always appear as pairs in the FPT, they are viewed as doublets. More precisely, they are called the Froissart doublets after Froissart who was the first to detect empirically this very useful phenomenon, which is unique to the versatile Padé methodology. By definition, noise is spurious information by which the genuine part of the signal is corrupted. Therefore, the pole-zero cancellation can be used to disentangle noise as an unphysical burden from the physical content in the considered signal, and this is the most important usage of the Froissart doublets in MRS, as well as in many other applications of the FPT.

The overall benefit from the concept of the Froissart doublets is illuminated in the present study within the FPT applied to the synthesized noise-free time signals. Spurious poles and zeros always appear, even in processing noiseless time signals by using any estimator. This occurs because the stable fundamental frequencies and amplitudes are typically reconstructed for overconditioned systems for which significantly more signal points are needed than the total number of unknown spectral parameters. The illustrations of the Froissart doublets necessitate the knowledge of both the zeros and the poles of the complex-valued spectrum in the form of the polynomial quotient. These spectral zeros and poles are obtained by solving the characteristic equations for the numerator and denominator polynomial, respectively. Overall, using the Argand diagrams, we found that the Froissart doublets are distributed along lines in the rectangular coordinates. These distributions are configured in a very regular and even fashion for the investigated noise-free time signal. The pole-zero cancellations occur systematically with a regular pattern, thus permitting a clear distinction between the spurious and genuine resonances. Such an unequivocal distinction allows the exact reconstruction of all the true values for the genuine spectral parameters, including the fundamental frequencies, the corresponding amplitudes and the original number of the physical resonances. The unique pole-zero cancellations for the Froissart doublets are simultaneously accompanied by the corresponding remarkable zero-valued amplitudes as yet another illustration of the FPT to distinguish genuine from spurious resonances.

Overall the FPT is shown to separate sharply the genuine from the spurious resonances in the two disjoint regions for positive and negative imaginary frequencies, respectively. Such an unprecedented separation of the physical from the nonphysical informational content of the investigated data by using the FPT is expected to play a key role in optimally reliable spectral analyses in all areas of signal processing across the inter-disciplinary fields, including the powerful applications of MRS to early cancer diagnostics and other aspects of clinical oncology.

Acknowledgments This work has been supported by King Gustav the 5th Jubilee Foundation, the Karolinska Institute Research Fund and the Signe and Olof Wallenius Stiftelse.

References

1. T. Bezabeh, O. Odlum, R. Nason, P. Kerr, D. Sutherland, R. Pael, I.C.P. Smith, Prediction of treatment response in head and neck cancer by magnetic resonance spectroscopy. Am. J. Neuroradiol. **26**, 2108 (2005)
2. P.J. Bolan, M.T. Nelson, D. Yee, M. Garwood, Imaging in breast cancer: magnetic resonance spectroscopy. Breast Cancer Res. **7**, 149 (2005)
3. J. Evelhoch, M. Garwood, D. Vigneron, M. Knopp, D. Sullivan, A. Menkens, et al., Expanding the use of magnetic resonance in the assessment of tumor response to therapy. Cancer Res. **65**, 7041 (2005)
4. W. Hollingworth, L.S. Medina, R.E. Lenkinski, D.K. Shibata, B. Bernal, D. Zurakowski, B. Comstock, J.G. Jarvik, A systematic literature review of magnetic resonance spectroscopy for the characterization of brain tumors. Am. J. Neuroradiol. **27**, 1404 (2006)
5. H. Hricak, MR imaging and MR spectroscopic imaging in the pre-treatment evaluation of prostate cancer. Br. J. Radiol. **78**, S103 (2005)
6. R. Huzjan, E. Sala, H. Hricak, Magnetic resonance imaging and magnetic resonance spectroscopic imaging of prostate cancer. Nat. Clin. Pract. Urol. **2**, 434 (2005)
7. A.D. King, D.K.W. Yeung, A.T. Ahuja, G.M.K. Tse, H.Y. Yuen, K.T. Wong, A.C. van Hasselt, Salivary gland tumors at in vivo MR spectroscopy. Radiology **237**, 563 (2005)
8. A.D. King, D.K.W. Yeung, A.T. Ahuja, G.M.K. Tse, A.B.W. Chan, S.S.L. Lam, A.C. van Hasselt, In vivo ^{1}H MR spectroscopy of thyroid cancer. Eur. J. Radiol. **54**, 112 (2005)
9. L. Kwock, J.K. Smith, M. Castillo, M.G. Ewend, F. Collichio, D.E. Morris, T.W. Bouldin, S. Cush, Clinical role of proton magnetic resonance spectroscopy in oncology: brain, breast and prostate cancer. Lancet Oncol. **7**, 859 (2006)
10. S. Katz, M. Rosen, MR imaging and MR spectroscopy in prostate cancer management. Radiol. Clin. N. Am. **44**, 723 (2006)
11. D. Mankoff, Imaging in breast cancer—revisited. Breast Cancer Res. **7**, 276 (2005)
12. G.S. Payne, M.O. Leach, Applications of magnetic resonance spectroscopy in radiotherapy treatment planning. Br. J. Radiol. **79**, S16 (2006)
13. N.A. Sibtain, F.A. Howe, D.E. Saunders, The clinical value of proton magnetic resonance spectroscopy in adult brain tumours. Clin. Radiol. **62**, 109 (2007)
14. K. Belkić, *Molecular Imaging through Magnetic Resonance for Clinical Oncology* (Cambridge International Science Publishing, Cambridge, 2004)
15. K. Belkić, Dž. Belkić, Spectroscopic imaging through magnetic resonance for brain tumour diagnostics. J. Comp. Method Sci. Eng. **4**, 157 (2004)
16. S. Nelson, Multivoxel magnetic resonance spectroscopy of brain tumors. Mol. Cancer Ther. **2**, 497 (2003)
17. F.A. Howe, K.S. Opstad, ^{1}H spectroscopy of brain tumors and masses. NMR Biomed. **16**, 123 (2003)
18. R. Dhingsa, A. Qayyum, F.V. Coakley, Y. Lu, K.D. Jones, M.G. Swanson, P.R. Carroll, H. Hricak, J. Kurhanewicz, Prostate cancer localization with endorectal MR imaging and MR spectroscopic imaging: effect of clinical data on reader accuracy. Radiology **230**, 215 (2004)
19. L. Bartella, E.A. Morris, D.D. Dershaw, L. Liberman, S.B. Thakur, C. Moskowitz, J. Guido, W. Huang, Proton MR spectroscopy with choline peak as malignancy marker improves positive predictive value for breast cancer diagnosis: preliminary study. Radiology **239**, 686 (2006)
20. N.R. Jagannathan, M. Kumar, V. Seenu, O. Coshic, S.N. Dwivedi, P.K. Julka, A. Srivastava, G.K. Rath, Evaluation of total choline from in-vivo volume localized proton MR spectroscopy and its response to neoadjuvant chemotherapy in locally advanced breast cancer. Br. J. Cancer **84**, 1016 (2001)
21. S. Meisamy, P.J. Bolan, E.H. Baker, R.L. Bliss, E. Gulbahce, L.I. Everson, M.T. Nelson, T.H. Emory, T.M. Tuttle, D. Yee, M. Garwood, Neoadjuvant chemotherapy of locally advanced breast cancer: predicting response with in vivo 1H MR spectroscopy—a pilot study at 4T. Radiology **233**, 424 (2004)
22. J.R. Stretch, R. Somorjai, R. Bourne, E. Hsiao, R.A. Scolyer, B. Dolenko, J.F. Thompson, C.E. Mountford, C.L. Lean, Melanoma metastases in regional lymph nodes are accurately detected by proton magnetic resonance spectroscopy of fine-needle aspirate biopsy samples. Ann. Surg. Oncol. **12**, 943 (2005)
23. K. Belkić, MR spectroscopic imaging in breast cancer detection: possibilities beyond the conventional theoretical framework for data analysis. Nucl. Instr. Method Phys. Res. A **525**, 313 (2004)

24. K. Belkić, Current dilemmas and future perspectives for breast cancer screening with a focus upon optimization of MR spectroscopic imaging by advances in signal processing. Isr. Med. Assoc. J. **6**, 610 (2004)
25. I. Gribbestad, B. Sitter, S. Lundgren, J. Krane, D. Axelson, Metabolite composition in breast tumors examined by proton nuclear MR spectroscopy. Anticancer Res. **19**, 1737 (1999)
26. R. Katz-Brull, P.T. Lavin, R.E. Lenkinski, Clinical utility of proton MR spectroscopy in characterizing breast lesions. J. Natl. Cancer Inst. **94**, 1197 (2002)
27. M. Kaminogo, H. Ishimaru, M. Morikawa, M. Ochi, R. Ushijima, M. Tani, Y. Matsuo, J. Kawakubo, S. Shibata, Diagnostic potential of short echo time MR spectroscopy of gliomas with single-voxel and point-resolved spatially localised proton spectroscopy of brain. Neuroradiology **43**, 353 (2001)
28. J. Griffiths, A.R. Tate, F.A. Howe, M. Stubbs, as part of the Multi-institutional group on MRS application to cancer. Magnetic resonance spectroscopy of cancer—practicalities of multi-centre trials and early results in non-Hodgkin's lymphoma. Eur. J. Cancer **38**, 2085 (2002)
29. I.C. Smith, D.E. Blandford, Diagnosis of cancer in humans by ^{1}H NMR of tissue biopsies. Biochem. Cell Biol. **76**, 472 (1998)
30. J.C. Wallace, G.P. Raaphorst, R.L. Somorjai, C.E. Ng, M. Fung Kee Fung, M. Senterman, I.C. Smith, Classification of ^{1}H MR spectra of biopsies from untreated and recurrent ovarian cancer using linear discriminant analysis. Magn. Reson. Med. **38**, 569 (1997)
31. E. Boss, S.H. Moolenaar, L.F.A.G. Massuger, H. Boonstra, U.F.H. Engelke, J.G.N. de Jong, R.A. Wevers, High-resolution proton nuclear magnetic resonance spectroscopy of ovarian cyst fluid. NMR Biomed. **13**, 297 (2000)
32. L.F.A.G. Massuger, P.B.J. van Vierzen, U. Engelke, A. Heerschap, ^{1}H-MR spectroscopy. A new technique to discriminate benign from malignant ovarian tumors. Cancer **82**, 1726 (1998)
33. Dž. Belkić, Fast Padé Transform (FPT) for magnetic resonance imaging and computerized tomography. Nucl. Instrum. Methods Phys. Res. A **471**, 165 (2001)
34. R. Wirestam, F. Ståhlberg, Wavelet-based noise reduction for improved deconvolution of time-series data in dynamic susceptibility-contrast MRI. MAGMA **18**, 113 (2005)
35. Dž. Belkić, *Quantum Mechanical Signal Processing and Spectral Analysis* (Institute of Physics Publishing, Bristol, 2004)
36. Dž. Belkić, K. Belkić, The fast Padé transform in magnetic resonance spectroscopy for potential improvements in early cancer diagnostics. Phys. Med. Biol. **50**, 4385 (2005)
37. Dž. Belkić, K. Belkić, Unequivocal disentangling genuine from spurious information in time signals: clinical relevance in cancer diagnostics through magnetic resonance spectroscopy. J. Math. Chem. doi:10.1007/s10910-007-9337-4
38. A. Maudsley, Can MR spectroscopy ever be simple and effective? Am. J. Neuroradiol. **69**, 2167 (2005)
39. C. Lanczos, *Applied Analysis* (Prentice-Hall, Englewood Cliffs, 1956)
40. A.A. Istratov, O.F. Virenko, Exponential analysis in physical phenomena. Rev. Sci. Instrum. **70**, 1233 (1999)
41. P.A. Bottomley, The trouble with spectroscopy papers. J. Magn. Reson. Imaging **2**, 1 (1992)
42. K.S. Opstad, S.W. Provencher, B.A. Bell, J.R. Griffiths, F.A. Howe, Detection of elevated glutathione in meningiomas by quantitative in vivo 1H MRS. Magn. Reson. Med. **49**, 632 (2003)
43. Y.-D. Cho, G.-H. Choi, S.-P. Lee, J.-K. Kim, ^{1}H-MRS metabolic patterns for distinguishing between meningiomas and other brain tumors. Magn. Reson. Imaging **21**, 663 (2003)
44. S.W. Provencher, Estimation of metabolite concentrations from localized in vivo proton NMR spectra Magn. Reson Med. **30**, 672 (1993)
45. E. Danielsen, B. Ross, *Magnetic Resonance Spectroscopy Diagnosis of Neurological Diseases* (Marcel Dekker, Inc., New York, 1999)
46. L. Brandão, R. Domingues, *MR Spectroscopy of the Brain* (Lippincott Williams & Wilkins, Philadelphia, 2004)
47. Dž. Belkić, Strikingly stable convergence of the fast Padé transform (FPT) for high-resolution parametric and non-parametric signal processing of Lorentzian and non-Lorentzian spectra. Nucl. Instrum. Methods Phys. Res. A **525**, 366 (2004)
48. Dž. Belkić, Error analysis through residual frequency spectra in the fast Padé transform (FPT). Nucl. Instrum. Methods Phys. Res. A **525**, 379 (2004)
49. Dž. Belkić, Analytical continuation by numerical means in spectral analysis using the fast Padé transform (FPT), Nucl. Instrum. Methods Phys. Res. A **525**, 372 (2004)

50. Dž. Belkić, Exact quantification of time signals in Padé-based magnetic resonance spectroscopy. Phys. Med. Biol. **51**, 2633 (2006)
51. Dž. Belkić, Exponential convergence rate (the spectral convergence) of the fast Padé transform for exact quantification in magnetic resonance spectroscopy. Phys. Med. Biol. **51**, 6483 (2006)
52. Dž. Belkić, K. Belkić, In vivo magnetic resonance spectroscopy by the fast Padé transform. Phys. Med. Biol. **51**, 1049 (2006)
53. M.F. Callaghan, D.J. Larkman, J.V. Hajnal, Padé methods for reconstruction and feature extraction in magnetic resonance imaging. Magn. Reson. Med. **54**, 1490 (2005)
54. Dž. Belkić, K. Belkić, Fast Padé transform for optimal quantification of time signals from magnetic resonance spectroscopy. Int. J. Quant. Chem. **105**, 493 (2005)
55. I. Tkáč, P. Andersen, G. Adriany, H. Merkle, K. Ugurbil, R. Gruetter, In vivo ^{1}H NMR spectroscopy of the human brain at 7T. Magn. Reson. Med. **46**, 451 (2001)
56. J. Frahm, H. Bruhn, M.L. Gyngell, K.D. Merboldt, W. Hanicke, R. Sauter, Localized high-resolution proton NMR spectroscopy using stimulated echoes: initial applications to human brain in vivo. Magn. Reson. Med. **9**, 79 (1989)
57. Dž. Belkić, K. Belkić, Mathematical modeling of an NMR chemistry problem in ovarian cancer diagnostics. J. Math. Chem. **43**, 395 (2008)
58. K. Belkić, Resolution performance of the fast Padé transform: potential advantages for magnetic resonance spectroscopy in ovarian cancer diagnostics. Nucl. Instrum. Meth. Phys. Res. A **580**, 874 (2007)
59. Dž. Belkić, K. Belkić, Decisive role of mathematical methods in early cancer diagnostics. J. Math. Chem. **42**, 1 (2007)
60. Dž. Belkić, Fast Padé transform for exact quantification of time signals in magnetic resonance spectroscopy. Adv. Quant. Chem. **51**, 157 (2006)
61. W.W.F. Pijnappel, A. van den Boogaart, R. de Beer, D. van Ormondt, SVD-based quantification of magnetic resonance signals. J. Magn. Reson. **97**, 122 (1992)
62. J.W.C. van der Veen, R. de Beer, P.R. Luyten, D. van Ormondt, Accurate quantification of in vivo 31P NMR signals using the variable projection method and prior knowledge. Magn. Reson. Med. **6**, 92 (1988)
63. L. Vanhamme, A. van den Boogaart, S. van Haffel, Improved method for accurate and efficient quantification of MRS data with use of prior knowledge. J. Magn. Reson. **29**, 35 (1997)
64. Dž. Belkić, Strikingly stable convergence of the fast Padé transform. J. Comp. Method Sci. Eng. **3**, 299 (2003)
65. Dž. Belkić, Padé-based magnetic resonance spectroscopy (MRS). J. Comp. Method Sci. Eng. **3**, 563 (2003)
66. Dž. Belkić, P.A. Dando, J. Main, H.S. Taylor, Three novel high-resolution nonlinear methods for fast signal processing. J. Chem. Phys. **113**, 6542 (2000)
67. V. Govindaraju, K. Young, A.A. Maudsley, Proton NMR chemical shifts and coupling constants for brain metabolites. NMR Biomed. **13**, 129 (2000)
68. P. Swindle, S. McCredie, P. Russell, U. Himmelreich, M. Khadra, C. Lean, C. Mountford, Pathologic characterization of human prostate tissue with proton MR spectroscopy. Radiology **228**, 144 (2003)
69. Dž. Belkić, Machine accurate quantification in magnetic resonance spectroscopy. Nucl. Instrum. Method Phys. Res. A **580**, 1034 (2007)
70. M. Froissart, Approximation de Padé: Application à la Physique des Particules Élémentaires, CNRS, RCP, Programme No. 25. Strasbourg **9**, 1 (1969)
71. F. Jolesz, Future of magnetic resonance imaging and magnetic resonance spectroscopy in oncology. ANZ J. Surg. **75**, 372 (2005)
72. C.E. Mountford, S. Doran, C. Lean, P. Russell, Proton MRS can determine the pathology of human cancers with a high level of accuracy. Chem. Rev. **104**, 3677 (2004)
73. Dž. Belkić, K. Belkić, Mathematical optimization of in vivo NMR chemistry through the fast Padé transform: potential relevance for early breast cancer detection by magnetic resonance spectroscopy. J. Math. Chem. **40**, 85 (2006)
74. E.O. Aboagye, Z.M. Bhujwalla, Malignant transformation alters membrane choline phospholipid metabolism of human mammary epithelial cells. Cancer Res. **59**, 80 (1999)
75. R. Katz-Brull, D. Seger, D Rivenson-Segal, E. Rushkin, H. Degani, Metabolic markers of breast cancer. Enhanced choline metabolism and reduced choline-ether-phospholipid synthesis. Cancer Res. **62**, 1966 (2002)

76. K. Glunde, C. Jie, Z.M. Bhujwalla, Molecular causes of the aberrant choline phospholipid metabolism in breast cancer. Cancer Res. **64**, 4270 (2004)
77. K. Belkić, Padé-optimized magnetic resonance spectroscopy: New possibilities for early breast cancer detection. Medicinteknikdagarna, October 2006, Uppsala
78. M. Kriege, C.T.M. Brekelmans, C. Boetes, P.E. Besnard, H.M. Zonderland, I.M. Obdeijn, et al., Efficacy of MRI and mammography for breast-cancer screening in women with a familial or genetic predisposition. N. Engl. J. Med. **351**, 427 (2004)
79. C.K. Kuhl, S. Scharding, C.C. Leutner, N. Markkabati-Spitz, E. Wardelmann, R. Fimmers, et al., Mammography, breast ultrasound, and magnetic resonance imaging for surveillance of women at high familial risk for breast cancer. J. Clin. Oncol. **23**, 8469 (2005)
80. J.A. Smith, E. Andreopoulou, An overview of the status of imaging screening technology for breast cancer. Ann. Oncol. **15**(Suppl. 1), i18 (2004)
81. Memorial Sloan-Kettering, cited by: T. Freeman, Medical PhysicsWeb.org Newswire Week 47, 2007
82. J. Kuranewicz, M.G. Swanson, S.J. Nelson, D.B. Vigneron, Combined magnetic resonance imaging and spectroscopic imaging approach to molecular imaging of prostate cancer. J. Magn. Reson. Imaging **16**, 451 (2002)
83. M.G. Swanson, A.S. Zektzer, Z.L. Tabatabai, J. Simko, S. Jarso, K.R. Keshari, L. Schmitt, P.R. Carroll, K. Shinohara, D.B. Vigneron, J. Kurhanewicz, Quantitative analysis of prostate metabolites using ^{1}H HR-MAS spectroscopy. Magn. Reson. Med. **55**, 1257 (2006)
84. A.P. Chen, C.H. Cunningham, J. Kurhanewicz, D. Xu, R.E. Hurd, J.M. Pauly, L. Carvajal, K. Karpodinis, D.B. Vigneron, High-resolution 3D MR spectroscopic imaging of the prostate at 3T with the MLEV-PRESS sequence. Magn. Reson. Imaging **24**, 825 (2006)
85. C.L. Lean, R. Bourne, J.F. Thompson, R.A. Scolyer, J. Stretch, L.X. Li, P. Russell, C. Mountford, Rapid detection of metastatic melanoma in lymph nodes using proton magnetic resonance spectroscopy of fine needle aspiration biopsy specimens. Melanoma Res. **13**, 259 (2003)
86. J.F. Thompson, J.R. Stretch, R.F. Uren, V.S. Ka, R.A. Scolyer, Sentinel node biopsy for melanoma: Where have we been and where are we going? Ann. Surg. Oncol. **11**(Suppl.), 147S (2004)
87. Dž. Belkić, K. Belkić, High-resolution magnetic resonance imaging (MRI), Medical Imaging Conference IEEE (MIC), Portland, October 22–25, 2003 Abstract Number 1971 (CD)
88. M.A. Thomas, N. Wyckoff, K. Yue, N. Binesh, S. Banakar, H-K. Chung, J. Sayre, N. DeBruhl, Two-dimensional MR spectroscopy characterization of breast cancer in vivo. Two-dimensional MR spectroscopy characterization of breast cancer in vivo. Technol. Cancer Res. Treat. **4**, 99 (2005)
89. Dž. Belkić, High-resolution parametric estimation of two-dimensional magnetic resonance spectroscopy, 20th Annual Meeting of European Soc. Magn. Res. Med. Biol. (ESMRMB), Abstract Number 365 (CD), Rotterdam (Netherlands), September 18–21, 2003
90. K. Belkić, Dž. Belkić. The fast Padé transform (FPT) for magnetic resonance spectroscopic imaging (MRSI) in oncology, Medical Imaging Conference IEEE (MIC), Portland, October 22–25, 2003 Abstract Number 1918 (CD), Portland (Oregon, USA), October 22–25, 2003
91. I. Park, G. Tamai, M.C. Lee, C.F. Chuang, S.M. Chang, M.S. Berger, S.J. Nelson, A. Pirzkall, Patterns of recurrence analysis in newly diagnosed glioblastoma multiforme after three-dimensional conformal radiation therapy with respect to pre-radiation therapy magnetic resonance spectroscopic findings. Int. J. Radiat. Oncol. Biol. Phys. **69**, 381 (2007)